PHYSICAL REVIEW D **88,** 083517 (2013)

Decomposing CMB lensing power with simulation

Ethan Anderes*

Statistics Department, University of California, Davis, California 95616, USA

(Received 11 January 2013; published 18 October 2013)

The reconstruction of the cosmic microwave background lensing potential is based on a Taylor expansion of lensing effects which is known to have poor convergence properties. For lensing of temperature fluctuations, an understanding of the higher order terms in this expansion which is accurate enough for current experimental sensitivity levels has been developed in Hanson *et al.* (2010), as well as a slightly modified Hu and Okamoto quadratic estimator which incorporates lensed rather than unlensed spectra into the estimator weights to mitigate the effect of higher order terms. We extend these results in several ways: (1) we generalize this analysis to the full set of quadratic temperature/polarization lensing estimators, (2) we study the effect of higher order terms for more futuristic experimental noise levels, (3) we show that the ability of the modified quadratic estimator to mitigate the effect of higher order terms relies on a delicate cancellation which occurs only when the true lensed spectra are known. We investigate the sensitivity of this cancellation to uncertainties in or knowledge of these spectra. We find that higher order terms in the Taylor expansion can impact projected error bars at experimental sensitivities similar to those found in future ACTpol/SPTpol experiments.

DOI: 10.1103/PhysRevD.88.083517 PACS numbers: 95.35.+d, 98.80.−k

I. INTRODUCTION

Over the past year, data from two ground based telescopes, ACT and SPT, have resulted in the first direct measurement of the weak lensing power spectrum solely from cosmic microwave background (CMB) measurements [1,2]. In the coming years, the data from Planck and upcoming experiments ACTpol and SPTpol will begin probing this lensing at much greater resolution. The state-of-the-art estimator of weak lensing, the quadratic estimator developed by Hu and Okamoto [3,4], works in part through a delicate cancellation of terms in a Taylor expansion of the lensing effect on the CMB. In this paper we present a simulation based approach for exploring the nature of this cancellation for both the CMB intensity and the polarization fields. In particular, we study a slightly modified quadratic estimator which incorporates lensed rather than unlensed spectra into the estimator weights to mitigate the effect of higher order terms and uses the observed lensed CMB fields to correct for the, so-called, $N_l^{(0)}$ bias.

The simulation methodology presented here allows a stochastic exploration of the higher order bias terms of the quadratic estimate and can be used to reduce the computational load associated with iterative debiasing algorithms for the quadratic estimate. In this paper, we use our simulation methodology to present a detailed study of the, so-called, $N_l^{(1)}$ and $N_l^{(2)}$ bias for the full set of quadratic temperature/polarization lensing estimators. The $N_l^{(1)}$ bias was first explored for the standard flat sky quadratic estimate in Kesden *et al.* [5]. For full sky CMB temperature maps, Hanson *et al.* [6] developed an approximation to the higher order bias terms, including $N_l^{(2)}$, which is accurate enough for current experimental sensitivity levels as well as for the slightly modified quadratic estimator which incorporates lensed rather than unlensed spectra into the estimator weights. We generalize this analysis to the full set of modified quadratic temperature/polarization lensing estimators and demonstrate that, indeed, the lensed spectra weights mitigate the combined higher order bias. However, this mitigation is obtained only by an increase in the magnitude of both $N_l^{(1)}$ and $N_l^{(2)}$ to the extent that they nearly cancel. We explore the extent to which this cancellation is sensitive to fiducial uncertainty in the way the lensed spectra weights are computed. We find that, under experimental conditions similar to those in future ACTpol and SPTpol experiments, the EB quadratic estimator is not sensitive to low l fiducial uncertainty whereas the EE and TE are sensitive to the point of degrading inferential power.

The remainder of the paper is organized as follows. In Secs. II, III, and IV we give an overview of the modified quadratic estimate, derive the spectral density of the quadratic estimate in terms of higher order bias terms, and discuss the estimation of the spectral density of the lensing potential. In Sec. V we present two simulation based methods for estimating the higher order bias terms. The first simulation method works exclusively for estimating $N_l^{(1)}$, and is mainly used to validate the second algorithm which can produce all higher order terms $N_l^{(j)}$ for $j \geq 1$. In Sec. VI we use these methods to study the higher order terms for experimental noise levels similar to those found in future ACTpol and SPTpol experiments. The paper concludes with the Appendix which gives fast Fourier transform (FFT) algorithms for computing the modified quadratic estimate. These algorithms extend the FFT techniques

*anderes@stat.ucdavis.edu.

 © 2013 American Physical Society

developed in [3] to the computation of all quadratic normalization constants and provides fast (nonstochastic) algorithms which extend the simulation techniques found in [1] for computing the "Gaussian bias" from the lensed CMB four-point function for all temperature/polarization quadratic estimators.

II. THE QUADRATIC ESTIMATOR

The effect of weak lensing is to simply remap the CMB temperature $T(\boldsymbol{x})$ and Stokes polarization fields $Q(\boldsymbol{x})$ and $U(\boldsymbol{x})$ for a flat sky coordinate system $\boldsymbol{x} \in \mathbb{R}^2$. Up to leading order, the remapping displacements are given by $\nabla\phi(\boldsymbol{x})$, where $\phi(\boldsymbol{x})$ denotes a lensing potential and is the planar projection of a three-dimensional gravitational potential (see [7]). Therefore, for any CMB field $X \in \{T, Q, U\}$ the corresponding lensed field can be written $X(\boldsymbol{x} + \nabla\phi(\boldsymbol{x}))$. For the remainder of the paper we let

$$\tilde{X}(\boldsymbol{x}) \equiv X(\boldsymbol{x} + \nabla\phi(\boldsymbol{x})) + N^X(\boldsymbol{x})$$

denote the corresponding lensed CMB field with additive independent experimental noise given by N^X (which includes a beam deconvolution). Using this notation the corresponding lensed E and B modes are given by $\tilde{E}_{\boldsymbol{l}} \equiv -\cos(2\varphi_{\boldsymbol{l}})\tilde{Q}_{\boldsymbol{l}} - \sin(2\varphi_{\boldsymbol{l}})\tilde{U}_{\boldsymbol{l}}$ and $\tilde{B}_{\boldsymbol{l}} \equiv \sin(2\varphi_{\boldsymbol{l}})\tilde{Q}_{\boldsymbol{l}} - \cos(2\varphi_{\boldsymbol{l}})\tilde{U}_{\boldsymbol{l}}$ where $X_{\boldsymbol{l}} \equiv \int \frac{d^2\boldsymbol{x}}{2\pi} e^{-i\boldsymbol{x}\cdot\boldsymbol{l}} X(\boldsymbol{x})$ (unitary angular frequency) and $\varphi_{\boldsymbol{l}}$ denotes the phase angle of frequency $\boldsymbol{l}$.

For any field X, $Y \in \{T, Q, U, E, B\}$ the spectral density $C_{\boldsymbol{l}}^{XY}$ is defined to satisfy $\langle X_{\boldsymbol{l}} Y^*_{\boldsymbol{l}'}\rangle = \delta_{\boldsymbol{l}-\boldsymbol{l}'} C_{\boldsymbol{l}}^{XY}$ where $\delta_{\boldsymbol{l}} \equiv \int \frac{d^2\boldsymbol{x}}{(2\pi)^2} e^{i\boldsymbol{x}\cdot\boldsymbol{l}}$. The angled brackets $\langle\cdot\rangle$ denote ensemble averaging (or expected value) over both the CMB fields and the large scale structure given by ϕ. In addition, we let $\langle\cdot\rangle_{XY}$ denote expected value with respect to the unlensed CMB fields T, Q, U, E, B and $\langle\cdot\rangle_\phi$ denote expected value with respect to large scale structure given by ϕ. Throughout this paper we stipulate that ϕ is independent of T, Q, U, E, B which implies $\langle\cdot\rangle = \langle\langle\cdot\rangle_{XY}\rangle_\phi$. We let $\tilde{C}_{\boldsymbol{l}}^{XY}$ denote the lensed CMB spectral density *without* experimental noise and let $C_{\boldsymbol{l},\mathrm{exp}}^{XY} \equiv C_{\boldsymbol{l}}^{XY} + C_{\boldsymbol{l}}^{N^X N^Y}$ and $\tilde{C}_{\boldsymbol{l},\mathrm{exp}}^{XY} \equiv \tilde{C}_{\boldsymbol{l}}^{XY} + C_{\boldsymbol{l}}^{N^X N^Y}$ denote the corresponding unlensed and lensed spectral densities *with* the additional experimental noise.

The quadratic estimate, based on two lensed CMB fields $\tilde{X}$ and $\tilde{Y}$, is derived from the following two statements:

$$\langle \tilde{X}_{\boldsymbol{k}+\boldsymbol{l}} \tilde{Y}^*_{\boldsymbol{k}}\rangle_{XY} \approx \phi_{\boldsymbol{l}} f_{\boldsymbol{l},\boldsymbol{k}}^{XY}, \quad \text{when } \boldsymbol{l} \neq 0; \tag{1}$$

$$\langle \tilde{X}_{\boldsymbol{k}+\boldsymbol{l}} \tilde{Y}^*_{\boldsymbol{k}}\rangle = \delta_{\boldsymbol{l}} \tilde{C}_{\boldsymbol{k},\mathrm{exp}}^{XY} \tag{2}$$

which hold for any X, $Y \in \{T, E, B\}$ and where the coefficients $f_{\boldsymbol{l},\boldsymbol{k}}^{XY}$ are given in the Appendix. Equation (1) approximates the cross frequency correlation (at separation lag $\boldsymbol{l}$) induced by the nonstationarity in $\tilde{X}$ (when regarding ϕ as a fixed nonrandom field). This is derived through a Taylor expansion of the lensing operation for any $X \in \{T, Q, U\}$

$$\tilde{X}(\boldsymbol{x}) = \delta^0 X(\boldsymbol{x}) + \delta^1 X(\boldsymbol{x}) + \delta^2 X(\boldsymbol{x}) + \cdots \tag{3}$$

where $\delta^0 X(\boldsymbol{x}) \equiv X(\boldsymbol{x}) + N^X(\boldsymbol{x})$, $\delta^1 X(\boldsymbol{x}) \equiv \nabla^a X(\boldsymbol{x}) \nabla_a \phi(\boldsymbol{x})$, etc. When $X \in \{E, B\}$ one defines $\delta^j E_{\boldsymbol{l}} \equiv -\cos(2\varphi_{\boldsymbol{l}})\delta^j Q_{\boldsymbol{l}} - \sin(2\varphi_{\boldsymbol{l}})\delta^j U_{\boldsymbol{l}}$ and $\delta^j B_{\boldsymbol{l}} \equiv \sin(2\varphi_{\boldsymbol{l}})\delta^j Q_{\boldsymbol{l}} - \cos(2\varphi_{\boldsymbol{l}})\delta^j U_{\boldsymbol{l}}$. Then by expanding $\tilde{X}_{\boldsymbol{k}+\boldsymbol{l}} \tilde{Y}^*_{\boldsymbol{k}}$ with (3), regrouping terms by the order of ϕ, one obtains $f_{\boldsymbol{l},\boldsymbol{k}}^{XY} \phi_{\boldsymbol{l}} = \langle \delta^1 X_{\boldsymbol{k}+\boldsymbol{l}} \delta^0 Y^*_{\boldsymbol{k}}\rangle_{XY} + \langle \delta^0 X_{\boldsymbol{k}+\boldsymbol{l}} \delta^1 Y^*_{\boldsymbol{k}}\rangle_{XY}$ which gives approximation (1). Equation (2), on the other hand, is obtained by treating both the CMB and the large scale structure ϕ as random so that $\tilde{X}$, from this viewpoint, is isotropic (but non-Gaussian).

Hu and Okamoto [3,4] used approximations (1) and (2) to construct the optimal quadratic estimate of ϕ based on $\tilde{X}$ and $\tilde{Y}$ as follows:

$$\hat{\phi}_{\boldsymbol{l}}^{XY} \equiv A_{\boldsymbol{l}}^{XY} \int \frac{d^2\boldsymbol{k}}{2\pi} g_{\boldsymbol{l},\boldsymbol{k}}^{XY} \tilde{X}_{\boldsymbol{k}+\boldsymbol{l}} \tilde{Y}^*_{\boldsymbol{k}} \tag{4}$$

where $g_{\boldsymbol{l},\boldsymbol{k}}^{XY} \equiv 2\pi f_{\boldsymbol{l},\boldsymbol{k}}^{XY} [\tilde{C}_{\boldsymbol{k}+\boldsymbol{l},\mathrm{exp}}^{XX} \tilde{C}_{\boldsymbol{k},\mathrm{exp}}^{YY}]^{-1}$. The normalizing constant $A_{\boldsymbol{l}}^{XY}$ is determined through an unbiased constraint. In particular, using the fact that $f_{\boldsymbol{l},\boldsymbol{k}}^{XY}$ is real we have that $\langle \hat{\phi}_{\boldsymbol{l}}^{XY}\rangle_{XY} = \phi_{\boldsymbol{l}} A_{\boldsymbol{l}}^{XY} \int \frac{d^2\boldsymbol{k}}{(2\pi)^2} |g_{\boldsymbol{l},\boldsymbol{k}}^{XY}|^2 \tilde{C}_{\boldsymbol{k}+\boldsymbol{l},\mathrm{exp}}^{XX} \tilde{C}_{\boldsymbol{k},\mathrm{exp}}^{YY}$ by Eq. (1). Then requiring that $\langle \hat{\phi}_{\boldsymbol{l}}^{XY}\rangle = \phi_{\boldsymbol{l}}$ determines $A_{\boldsymbol{l}}^{XY}$ as follows:

$$A_{\boldsymbol{l}}^{XY} = \left[\int \frac{d^2\boldsymbol{k}}{(2\pi)^2} |g_{\boldsymbol{l},\boldsymbol{k}}^{XY}|^2 \tilde{C}_{\boldsymbol{k}+\boldsymbol{l},\mathrm{exp}}^{XX} \tilde{C}_{\boldsymbol{k},\mathrm{exp}}^{YY} \right]^{-1}. \tag{5}$$

Remark: Our notation for expressing the quadratic estimate in (4) is slightly different than that given in Hu [3]. The main difference is that the quadratic estimator in (4) integrates $\tilde{X}_{\boldsymbol{k}+\boldsymbol{l}} \tilde{Y}^*_{\boldsymbol{k}}$ over $\boldsymbol{k}$ to emphasize that, to estimate $\phi_{\boldsymbol{l}}$, the quadratic estimator cross correlates frequencies which are separated by lag $\boldsymbol{l}$. Moreover, to utilize a FFT characterization of $\hat{\phi}_{\boldsymbol{l}}^{TE}$ we use the slightly suboptimal estimator recommended on page 5 in [4]. Other than this simple notational difference and small change in $\hat{\phi}_{\boldsymbol{l}}^{TE}$, the quadratic estimates given by (4) are the same as those given in Hu [3].

A. Lensed versus unlensed weights

There is a small modification to the standard quadratic estimate $\hat{\phi}_{\boldsymbol{l}}^{XY}$ which can mitigate the low l bias [arising from the $N_{\boldsymbol{l}}^{(2)}$ term discussed in the next section] when using the observed power $|\hat{\phi}_{\boldsymbol{l}}^{XY}|^2$ to estimate $C_{\boldsymbol{l}}^{\phi\phi}$. This modified estimate, denoted $\tilde{\phi}_{\boldsymbol{l}}^{XY}$, is obtained by replacing all occurrences of unlensed spectra in $g_{\boldsymbol{l},\boldsymbol{k}}^{XY}$ and $A_{\boldsymbol{l}}^{XY}$ with the corresponding lensed spectra. In particular $\tilde{\phi}_{\boldsymbol{l}}^{XY}$ is defined as

$$\tilde{\phi}_{\boldsymbol{l}}^{XY} \equiv \tilde{A}_{\boldsymbol{l}}^{XY} \int \frac{d^2\boldsymbol{k}}{2\pi} \tilde{g}_{\boldsymbol{l},\boldsymbol{k}}^{XY} \tilde{X}_{\boldsymbol{k}+\boldsymbol{l}} \tilde{Y}^*_{\boldsymbol{k}} \tag{6}$$

where $\tilde{A}_{\boldsymbol{l}}^{XY} = [\int \frac{d^2\boldsymbol{k}}{(2\pi)^2} |\tilde{g}_{\boldsymbol{l},\boldsymbol{k}}^{XY}|^2 \tilde{C}_{\boldsymbol{k}+\boldsymbol{l},\mathrm{exp}}^{XX} \tilde{C}_{\boldsymbol{k},\mathrm{exp}}^{YY}]^{-1}$ and $\tilde{g}_{\boldsymbol{l},\boldsymbol{k}}^{XY}$ is obtained from $g_{\boldsymbol{l},\boldsymbol{k}}^{XY}$ by replacing every occurrence of $C_{\boldsymbol{l}}^{XY}$, $C_{\boldsymbol{l}}^{XX}$ and $C_{\boldsymbol{l}}^{YY}$ with the corresponding lensed spectra $\tilde{C}_{\boldsymbol{l}}^{XY}$, $\tilde{C}_{\boldsymbol{l}}^{XX}$ and $\tilde{C}_{\boldsymbol{l}}^{YY}$. For example, when $X = Y = T$ one has

$$g^{TT}_{\boldsymbol{l},\boldsymbol{k}} \equiv \frac{\boldsymbol{l}\cdot[(\boldsymbol{k}+\boldsymbol{l})C^{TT}_{\boldsymbol{k}+\boldsymbol{l}} - \boldsymbol{k}C^{TT}_{\boldsymbol{k}}]}{\tilde{C}^{TT}_{\boldsymbol{k}+\boldsymbol{l},\mathrm{exp}}\tilde{C}^{TT}_{\boldsymbol{k},\mathrm{exp}}};$$

$$\tilde{g}^{TT}_{\boldsymbol{l},\boldsymbol{k}} \equiv \frac{\boldsymbol{l}\cdot[(\boldsymbol{k}+\boldsymbol{l})\tilde{C}^{TT}_{\boldsymbol{k}+\boldsymbol{l}} - \boldsymbol{k}\tilde{C}^{TT}_{\boldsymbol{k}}]}{\tilde{C}^{TT}_{\boldsymbol{k}+\boldsymbol{l},\mathrm{exp}}\tilde{C}^{TT}_{\boldsymbol{k},\mathrm{exp}}}.$$

Notice that the estimate $\tilde{\phi}^{XY}_{\boldsymbol{k}}$ is not normalized to be unbiased. Indeed from Eq. (1) one has

$$\langle\tilde{\phi}^{XY}_{\boldsymbol{l}}\rangle_{XY} \approx \phi_{\boldsymbol{l}}\underbrace{\left[\tilde{A}^{XY}_{\boldsymbol{l}}\int\frac{d^2\boldsymbol{k}}{(2\pi)^2}\tilde{g}^{XY}_{\boldsymbol{l},\boldsymbol{k}}g^{XY}_{\boldsymbol{l},\boldsymbol{k}}\tilde{C}^{XX}_{\boldsymbol{k}+\boldsymbol{l},\mathrm{exp}}\tilde{C}^{YY}_{\boldsymbol{k},\mathrm{exp}}\right]}_{\equiv B^{XY}_{\boldsymbol{l}}}.$$

III. THE SPECTRAL DENSITY OF THE QUADRATIC ESTIMATE

In this section we derive the following all-order decomposition of the spectral density of the quadratic estimate:

$$\langle\hat{\phi}^{XY}_{\boldsymbol{l}}\hat{\phi}^{XY^*}_{\boldsymbol{l}'}\rangle = \delta_{\boldsymbol{l}-\boldsymbol{l}'}[C^{\phi\phi}_{\boldsymbol{l}} + N^{(0)}_{\boldsymbol{l}} + N^{(1)}_{\boldsymbol{l}} + \cdots] \quad (7)$$

which will then be used, in a subsequent section, to derive the estimation bias for $C^{\phi\phi}_{\boldsymbol{l}}$. The first term $N^{(0)}_{\boldsymbol{l}}$ is related to the disconnected terms of the lensed CMB four-point function, whereas the higher order terms $N^{(j)}_{\boldsymbol{l}}$ for $j \geq 1$ are related to the connected terms of the four-point function segmented by the order of $C^{\phi\phi}_{\boldsymbol{l}}$. Most of this section focuses on the quadratic estimate $\hat{\phi}^{XY}$ followed by a brief discussion of the corresponding decomposition for the modified quadratic estimate $\tilde{\phi}^{XY}$.

Our derivation of the spectral density of $\hat{\phi}^{XY}_{\boldsymbol{l}}$ in the flat sky is similar to the analysis of the full sky trispectrum done in Hanson *et al.* [6]. One starts by relating $\langle\hat{\phi}^{XY}_{\boldsymbol{l}}\hat{\phi}^{XY^*}_{\boldsymbol{l}'}\rangle$ to the lensed CMB four-point function by distributing the expected value as follows:

$$\langle\hat{\phi}^{XY}_{\boldsymbol{l}}\hat{\phi}^{XY^*}_{\boldsymbol{l}'}\rangle = A^{XY}_{\boldsymbol{l}}A^{XY}_{\boldsymbol{l}'}\int\frac{d^2\boldsymbol{k}}{2\pi}\int\frac{d^2\boldsymbol{k}'}{2\pi}g^{XY}_{\boldsymbol{l},\boldsymbol{k}}g^{XY}_{\boldsymbol{l}',\boldsymbol{k}'}\langle\tilde{X}_{\boldsymbol{k}+\boldsymbol{l}}\tilde{Y}^*_{\boldsymbol{k}}\tilde{X}^*_{\boldsymbol{k}'+\boldsymbol{l}'}\tilde{Y}_{\boldsymbol{k}'}\rangle. \quad (8)$$

To decompose (8) one then expands the four-point product term in the above integrand by expanding the lensed CMB Taylor expansion (3) to obtain

$$\langle\tilde{X}_{\boldsymbol{k}+\boldsymbol{l}}\tilde{Y}^*_{\boldsymbol{k}}\tilde{X}^*_{\boldsymbol{k}'+\boldsymbol{l}'}\tilde{Y}_{\boldsymbol{k}'}\rangle = \underbrace{\sum_{i,j,p,q}\langle\delta^iX_{\boldsymbol{k}+\boldsymbol{l}}\delta^jY^*_{\boldsymbol{k}}\delta^pX^*_{\boldsymbol{k}'+\boldsymbol{l}'}\delta^qY_{\boldsymbol{k}'}\rangle}_{\begin{array}{c}\mathit{decomposes\ further\ into\ connected}\\ \mathit{and\ disconnected\ terms}\end{array}}. \quad (9)$$

A. Disconnected terms

After distributing the expected value in the right-hand side of (9) through the j-fold convolution which makes up $\delta^jX_{\boldsymbol{l}}$ and subsequently applying Wicks theorem, one can further decompose $\langle\delta^iX_{\boldsymbol{k}+\boldsymbol{l}}\delta^jY^*_{\boldsymbol{k}}\delta^pX^*_{\boldsymbol{k}'+\boldsymbol{l}'}\delta^qY_{\boldsymbol{k}'}\rangle$ into what are called connected and disconnected terms. The disconnected terms in the four-point product are the terms which factor into cross-spectra of the fields δ^iX, δ^jX, δ^pX and δ^qX. For example, if $(i,j,p,q) = (1,1,0,0)$ and ϕ is assumed independent of X and Y then

$$\begin{aligned}&\langle\delta^1X_{\boldsymbol{k}+\boldsymbol{l}}\delta^1Y^*_{\boldsymbol{k}}\delta^0X^*_{\boldsymbol{k}'+\boldsymbol{l}'}\delta^0Y_{\boldsymbol{k}'}\rangle\\ &= \langle\delta^1X_{\boldsymbol{k}+\boldsymbol{l}}\delta^1Y^*_{\boldsymbol{k}}\ \delta^0X^*_{\boldsymbol{k}'+\boldsymbol{l}'}\delta^0Y_{\boldsymbol{k}'}\rangle \leftarrow \mathit{disconnected\ term}\\ &\quad + \langle\delta^1X_{\boldsymbol{k}+\boldsymbol{l}}\delta^1Y^*_{\boldsymbol{k}}\ \delta^0X^*_{\boldsymbol{k}'+\boldsymbol{l}'}\delta^0Y_{\boldsymbol{k}'}\rangle \leftarrow \mathit{connected\ term}\\ &\quad + \langle\delta^1X_{\boldsymbol{k}+\boldsymbol{l}}\delta^1Y^*_{\boldsymbol{k}}\ \delta^0X^*_{\boldsymbol{k}'+\boldsymbol{l}'}\delta^0Y_{\boldsymbol{k}'}\rangle \leftarrow \mathit{connected\ term}\end{aligned}$$

where the top contraction symbols correspond to pairing the CMB fields and the bottom contraction symbols correspond to pairing the lensing potential in δ^1X and δ^1Y. The contraction pairings on the above disconnected term results in a product of two spectra as follows:

$$\begin{aligned}&\langle\delta^1X_{\boldsymbol{k}+\boldsymbol{l}}\delta^1Y^*_{\boldsymbol{k}}\ \delta^0X^*_{\boldsymbol{k}'+\boldsymbol{l}'}\ \delta^0Y_{\boldsymbol{k}'}\rangle\\ &\quad = \langle\delta^1X_{\boldsymbol{k}+\boldsymbol{l}}\delta^1Y^*_{\boldsymbol{k}}\rangle\langle\delta^0X^*_{\boldsymbol{k}'+\boldsymbol{l}'}\ \delta^0Y_{\boldsymbol{k}'}\rangle.\end{aligned}$$

In a similar manner, for general (i,j,p,q), the disconnected terms can be grouped into the three types: one for each possible configuration of the top contraction symbols. Then regrouping all disconnected terms in (9), by top contraction type, results in the following three terms:

$$\begin{aligned}&\mathit{disconnected\ terms\ in}\sum_{i,j,p,q}\langle\delta^iX_{\boldsymbol{k}+\boldsymbol{l}}\delta^jY^*_{\boldsymbol{k}}\delta^pX^*_{\boldsymbol{k}'+\boldsymbol{l}'}\delta^qY_{\boldsymbol{k}'}\rangle\\ &= \langle\tilde{X}_{\boldsymbol{k}+\boldsymbol{l}}\tilde{Y}^*_{\boldsymbol{k}}\tilde{X}^*_{\boldsymbol{k}'+\boldsymbol{l}'}\tilde{Y}_{\boldsymbol{k}'}\rangle + \langle\tilde{X}_{\boldsymbol{k}+\boldsymbol{l}}\tilde{Y}^*_{\boldsymbol{k}}\tilde{X}^*_{\boldsymbol{k}'+\boldsymbol{l}'}\tilde{Y}_{\boldsymbol{k}'}\rangle\\ &\quad + \underbrace{\langle\tilde{X}_{\boldsymbol{k}+\boldsymbol{l}}\tilde{Y}^*_{\boldsymbol{k}}\tilde{X}^*_{\boldsymbol{k}'+\boldsymbol{l}'}\tilde{Y}_{\boldsymbol{k}'}\rangle}_{=0\ \text{when}\ \boldsymbol{l}\neq 0\ \text{or}\ \boldsymbol{l}'\neq 0}\\ &= \tilde{C}^{XY}_{\boldsymbol{k}+\boldsymbol{l},\mathrm{exp}}\tilde{C}^{XY}_{\boldsymbol{k},\mathrm{exp}}\delta_{\boldsymbol{k}+\boldsymbol{k}'+\boldsymbol{l}'}\delta_{\boldsymbol{k}+\boldsymbol{k}'+\boldsymbol{l}}\\ &\quad + \tilde{C}^{XX}_{\boldsymbol{k}+\boldsymbol{l},\mathrm{exp}}\tilde{C}^{YY}_{\boldsymbol{k},\mathrm{exp}}\delta_{\boldsymbol{k}-\boldsymbol{k}'}\delta_{\boldsymbol{k}+\boldsymbol{l}-\boldsymbol{k}'-\boldsymbol{l}'} \quad (10)\end{aligned}$$

where the last line is obtained by applying approximation (2). Substituting the four-point product term in (8) with (10) results in, what is typically called, the $N^{(0)}_{\boldsymbol{l}}$ bias:

$$\mathit{disconnected\ terms\ in}\langle\hat{\phi}^{XY}_{\boldsymbol{l}}\hat{\phi}^{XY^*}_{\boldsymbol{l}'}\rangle = \delta_{\boldsymbol{l}-\boldsymbol{l}'}N^{(0)}_{\boldsymbol{l}}$$

where

$$\begin{aligned}N^{(0)}_{\boldsymbol{l}} \equiv [A^{XY}_{\boldsymbol{l}}]^2\int\frac{d^2\boldsymbol{k}}{(2\pi)^2}&(g^{XY}_{\boldsymbol{l},\boldsymbol{k}}g^{XY}_{\boldsymbol{l},-\boldsymbol{k}-\boldsymbol{l}}\tilde{C}^{XY}_{\boldsymbol{k}+\boldsymbol{l},\mathrm{exp}}\tilde{C}^{XY}_{\boldsymbol{k},\mathrm{exp}}\\ &+ |g^{XY}_{\boldsymbol{l},\boldsymbol{k}}|^2\tilde{C}^{XX}_{\boldsymbol{k}+\boldsymbol{l},\mathrm{exp}}\tilde{C}^{YY}_{\boldsymbol{k},\mathrm{exp}}).\end{aligned}$$

B. Connected terms

The connected terms decompose further into what we call the "first connected terms" and the "second connected terms." There are only four first connected terms and they are defined as follows:

$$\begin{aligned}
&\textit{first connected terms in} \sum_{i,j,p,q} \langle \delta^i X_{\boldsymbol{k}+\boldsymbol{l}} \delta^j Y^*_{\boldsymbol{k}} \delta^p X^*_{\boldsymbol{k}'+\boldsymbol{l}'} \delta^q Y_{\boldsymbol{k}'} \rangle \\
&\equiv \langle \delta^1 \overbrace{X_{\boldsymbol{k}+\boldsymbol{l}} \delta^0 Y^*_{\boldsymbol{k}}}\, \delta^1 \overbrace{X^*_{\boldsymbol{k}'+\boldsymbol{l}'} \delta^0 Y_{\boldsymbol{k}'}} \rangle \\
&\quad + \langle \delta^1 \overbrace{X_{\boldsymbol{k}+\boldsymbol{l}} \delta^0 Y^*_{\boldsymbol{k}}}\, \delta^0 \overbrace{X^*_{\boldsymbol{k}'+\boldsymbol{l}'} \delta^1 Y_{\boldsymbol{k}'}} \rangle \\
&\quad + \langle \delta^0 \overbrace{X_{\boldsymbol{k}+\boldsymbol{l}} \delta^1 Y^*_{\boldsymbol{k}}}\, \delta^1 \overbrace{X^*_{\boldsymbol{k}'+\boldsymbol{l}'} \delta^0 Y_{\boldsymbol{k}'}} \rangle \\
&\quad + \langle \delta^0 \overbrace{X_{\boldsymbol{k}+\boldsymbol{l}} \delta^1 Y^*_{\boldsymbol{k}}}\, \delta^0 \overbrace{X^*_{\boldsymbol{k}'+\boldsymbol{l}'} \delta^1 Y_{\boldsymbol{k}'}} \rangle \\
&= \delta_{\boldsymbol{l}-\boldsymbol{l}'} f^{XY}_{\boldsymbol{l},\boldsymbol{k}} f^{XY}_{\boldsymbol{l}',\boldsymbol{k}'} C_{\boldsymbol{l}}^{\phi\phi}.
\end{aligned}$$

Then, by substituting the four-point product term in (8) with the first connected terms, one gets

$$\textit{first connected terms in} \langle \hat{\phi}^{XY}_{\boldsymbol{l}} \hat{\phi}^{XY^*}_{\boldsymbol{l}'} \rangle = \delta_{\boldsymbol{l}-\boldsymbol{l}'} C_{\boldsymbol{l}}^{\phi\phi}. \quad (11)$$

The remaining connected terms in the four-point product of (8), called second connected terms, are then regrouping corresponding to the order of ϕ. After noticing that any term of order ϕ^{2j+1} has expected value zero one obtains the following expansion:

$$\begin{aligned}
&\textit{second connected terms in} \langle \hat{\phi}^{XY}_{\boldsymbol{l}} \hat{\phi}^{XY^*}_{\boldsymbol{l}'} \rangle \\
&\quad = \delta_{\boldsymbol{l}-\boldsymbol{l}'} [N^{(1)}_{\boldsymbol{l}} + N^{(2)}_{\boldsymbol{l}} + \cdots]
\end{aligned}$$

where $N^{(j)}_{\boldsymbol{l}}$ is of order ϕ^{2j}. Putting all disconnected and connected terms together gives the desired expansion (7).

For reasons which will become clear in the next section, we define $N^{(1)}_{\boldsymbol{l}}$ in a slightly different, but equivalent, way that extends more naturally to the modified quadratic estimate. In particular, instead of defining $N^{(1)}_{\boldsymbol{l}}$ as the total contribution of the second connected terms in (8) of order ϕ^2, we define $N^{(1)}_{\boldsymbol{l}}$ simply as the total contribution of *all* connected terms of order ϕ^2 minus $C_{\boldsymbol{l}}^{\phi\phi}$.

C. The lensed weights

For the modified quadratic estimator, $\tilde{\phi}^{XY}_{\boldsymbol{l}}$, one can derive the expansion (7) with a few minor adjustments. In particular, the disconnected terms can be written

$$\textit{disconnected terms in} \langle \tilde{\phi}^{XY}_{\boldsymbol{l}} \tilde{\phi}^{XY^*}_{\boldsymbol{l}'} \rangle = \delta_{\boldsymbol{l}-\boldsymbol{l}'} N^{(0)}_{\boldsymbol{l}}$$

where

$$\begin{aligned}
N^{(0)}_{\boldsymbol{l}} \equiv [\tilde{A}^{XY}_{\boldsymbol{l}}]^2 \int \frac{d^2\boldsymbol{k}}{(2\pi)^2} (&\tilde{g}^{XY}_{\boldsymbol{l},\boldsymbol{k}} \tilde{g}^{XY}_{\boldsymbol{l},-\boldsymbol{k}-\boldsymbol{l}} \tilde{C}^{XY}_{\boldsymbol{k}+\boldsymbol{l},\mathrm{exp}} \tilde{C}^{XY}_{\boldsymbol{k},\mathrm{exp}} \\
&+ |\tilde{g}^{XY}_{\boldsymbol{l},\boldsymbol{k}}|^2 \tilde{C}^{XX}_{\boldsymbol{k}+\boldsymbol{l},\mathrm{exp}} \tilde{C}^{YY}_{\boldsymbol{k},\mathrm{exp}}).
\end{aligned}$$

The first connected terms are slightly different due to the intentional bias in the modified quadratic estimate yielding

$$\textit{first connected terms in} \langle \tilde{\phi}^{XY}_{\boldsymbol{l}} \tilde{\phi}^{XY^*}_{\boldsymbol{l}'} \rangle = \delta_{\boldsymbol{l}-\boldsymbol{l}'} [B^{XY}_{\boldsymbol{l}}]^2 C_{\boldsymbol{l}}^{\phi\phi}.$$

After these adjustments are made the remaining terms $N^{(j)}_{\boldsymbol{l}}$ are defined exactly the same way as for $\hat{\phi}^{XY}_{\boldsymbol{l}}$: when $j \geq 2$, $N^{(j)}_{\boldsymbol{l}}$ is defined as the total contribution of the connected terms in (8) which are order ϕ^{2j}; and $N^{(1)}_{\boldsymbol{l}}$ as the total contribution of the connected terms in (8) which are order ϕ^2 minus $C_{\boldsymbol{l}}^{\phi\phi}$. This is consistent with the previous definition of $N^{(j)}_{\boldsymbol{l}}$ for $\hat{\phi}^{XY}_{\boldsymbol{l}}$ and preserves the natural expansion

$$\langle \tilde{\phi}^{XY}_{\boldsymbol{l}} \tilde{\phi}^{XY^*}_{\boldsymbol{l}'} \rangle = \delta_{\boldsymbol{l}-\boldsymbol{l}'} [C_{\boldsymbol{l}}^{\phi\phi} + N^{(0)}_{\boldsymbol{l}} + N^{(1)}_{\boldsymbol{l}} + \cdots]. \quad (12)$$

IV. ESTIMATION OF $C_{\boldsymbol{l}}^{\boldsymbol{\phi\phi}}$

In this section we show how the expansions (7) and (12) are used to derive and analyze estimates of $C_{\boldsymbol{l}}^{\phi\phi}$. In what follows, we give a detailed derivation of our results for the regular quadratic estimate $\hat{\phi}^{XY}_{\boldsymbol{l}}$ and simply remark that the same results can be similarly derived for modified quadratic estimate $\tilde{\phi}^{XY}_{\boldsymbol{l}}$.

For current experimental conditions the first term $N^{(0)}_{\boldsymbol{l}}$ dominates the sum $\sum_{j=0}^{\infty} N^{(j)}_{\boldsymbol{l}}$. Therefore a natural bias-corrected estimate of $C_{\boldsymbol{l}}^{\phi\phi}$ is given by $\delta_0^{-1} |\hat{\phi}^{XY}_{\boldsymbol{l}}|^2 - N^{(0)}_{\boldsymbol{l}}$. Notice, however, that to compute $N^{(0)}_{\boldsymbol{l}}$ one needs a model for the lensed spectra with experimental noise: $\tilde{C}^{XX}_{\boldsymbol{l},\mathrm{exp}}$, $\tilde{C}^{YY}_{\boldsymbol{l},\mathrm{exp}}$ and $\tilde{C}^{XY}_{\boldsymbol{l},\mathrm{exp}}$. This normally requires knowledge of the very quantity we are estimating: $C_{\boldsymbol{l}}^{\phi\phi}$. One way to circumvent this difficulty is to replace the experimental lensed spectrums with estimates from the observations $\tilde{X}$ and $\tilde{Y}$. This results in the *observed* $N^{(0)}_{\boldsymbol{l}}$ bias and is given by

$$\begin{aligned}
N^{(0)}_{\boldsymbol{l},\mathrm{obs}} \equiv \delta_0^{-2} [A^{XY}_{\boldsymbol{l}}]^2 \int \frac{d^2\boldsymbol{k}}{(2\pi)^2} (&g^{XY}_{\boldsymbol{l},\boldsymbol{k}} g^{XY}_{\boldsymbol{l},-\boldsymbol{k}-\boldsymbol{l}} \tilde{X}_{\boldsymbol{k}+\boldsymbol{l}} \tilde{Y}^*_{\boldsymbol{k}+\boldsymbol{l}} \tilde{X}_{\boldsymbol{k}} \tilde{Y}^*_{\boldsymbol{k}} \\
&+ |g^{XY}_{\boldsymbol{l},\boldsymbol{k}}|^2 |\tilde{X}_{\boldsymbol{k}+\boldsymbol{l}}|^2 |\tilde{Y}_{\boldsymbol{k}}|^2).
\end{aligned}$$

Using $N^{(0)}_{\boldsymbol{l},\mathrm{obs}}$ in place of $N^{(0)}_{\boldsymbol{l}}$ yields $\delta_0^{-1} |\hat{\phi}^{XY}_{\boldsymbol{l}}|^2 - N^{(0)}_{\boldsymbol{l},\mathrm{obs}}$ as an estimate of $C_{\boldsymbol{l}}^{\phi\phi}$ which does require knowledge of $C_{\boldsymbol{l}}^{\phi\phi}$ to compute it.

Remark: To be clear on nomenclature, we say that a fixed estimator $\hat{C}_{\boldsymbol{l}}^{\phi\phi}$ of $C_{\boldsymbol{l}}^{\phi\phi}$ is said to be *unbiased* if $\langle \hat{C}_{\boldsymbol{l}}^{\phi\phi} \rangle - C_{\boldsymbol{l}}^{\phi\phi} = 0$ uniformly over all possible values of the unknown spectral density $C_{\boldsymbol{l}}^{\phi\phi}$. A *biased* estimator, on the other hand, is one for which there exists some $C_{\boldsymbol{l}}^{\phi\phi}$ such that $\langle \hat{C}_{\boldsymbol{l}}^{\phi\phi} \rangle - C_{\boldsymbol{l}}^{\phi\phi} \neq 0$. In this case, the term *estimation bias* then refers to the quantity $\langle \hat{C}_{\boldsymbol{l}}^{\phi\phi} \rangle - C_{\boldsymbol{l}}^{\phi\phi}$ as a function of $C_{\boldsymbol{l}}^{\phi\phi}$. Notice that for $\hat{C}_{\boldsymbol{l}}^{\phi\phi}$ to be considered an estimator it must be a function of the observable data only and can depend on $C_{\boldsymbol{l}}^{\phi\phi}$ only implicitly through the statistical

model of the data. It may directly depend on a fiducial guess of $C_l^{\phi\phi}$ but this fiducial guess must be fixed and the simulation truth $C_l^{\phi\phi}$ must vary when computing the bias. It is under this context that we analyze the quadratic estimator.

Remark: Up to this point we have been assuming an infinite sky when computing the Fourier transform $\int \frac{d^2\boldsymbol{x}}{2\pi} e^{-i\boldsymbol{l}\cdot\boldsymbol{x}}$. However, the above Fourier transforms will typically be done on a pixelized periodic finite sky. In this case, δ_0 is approximated as $1/\Delta\boldsymbol{l}$ where $\Delta\boldsymbol{l}$ is the area element of the grid in Fourier space induced by finite area sky. For the remainder of the paper we do not distinguish the finite versus infinite case and simply equate δ_0 with $1/\Delta\boldsymbol{l}$ leaving it understood that equality holds in the limit as $\Delta\boldsymbol{l} \to 0$.

A. The bias of $\delta_0^{-1}|\hat{\phi}_l^{XY}|^2 - N_{l,\mathrm{obs}}^{(0)}$

We will derive three main expansions, which decompose the bias: $\langle \delta_0^{-1}|\hat{\phi}_l^{XY}|^2 - N_{l,\mathrm{obs}}^{(0)}\rangle - C_l^{\phi\phi}$ (and similar definitions for the modified quadratic estimate). These expansions will be denoted as follows:

$$\hat{\phi}_l^{XY} = \mathcal{L}_l^{(0)} + \mathcal{L}_l^{(1)} + \mathcal{L}_l^{(2)} + \cdots \tag{13}$$

$$|\hat{\phi}_l^{XY}|^2 = \mathcal{O}_l^{(0)} + \mathcal{O}_l^{(1)} + \mathcal{O}_l^{(2)} + \cdots \tag{14}$$

$$N_{l,\mathrm{obs}}^{(0)} = \mathcal{N}_l^{(0)} + \mathcal{N}_l^{(1)} + \mathcal{N}_l^{(2)} + \cdots \tag{15}$$

where the terms $\mathcal{L}_l^{(j)}$, $\mathcal{O}_l^{(j)}$ and $\mathcal{N}_l^{(j)}$ are each of order j in ϕ. Expansions (13)–(15) are all obtained by expanding $\tilde{X}_{\boldsymbol{k}}$ and $\tilde{Y}_{\boldsymbol{k}}$ using (3) then regrouping the terms by the order of ϕ. This expansion and subsequent regrouping yields the following analytic expressions for each term:

$$\mathcal{L}_l^{(j)} \equiv \sum_{p=0}^{j} A_l^{XY} \int \frac{d^2\boldsymbol{k}}{2\pi} g_{l,k}^{XY}[\delta^p X_{k+l}\delta^{j-p}Y_k^*];$$

$$\mathcal{O}_l^{(j)} \equiv \sum_{p=0}^{j} \mathcal{L}_l^{(p)}\mathcal{L}_l^{(j-p)^*};$$

$$\mathcal{N}_l^{(j)} \equiv \sum_{p=0}^{j} \delta_0^{-2}[A_l^{XY}]^2 \int \frac{d^2\boldsymbol{k}}{(2\pi)^2}(g_{l,k}^{XY} g_{l,-k-l}^{XY}\mathcal{P}_{k+l}^{XY,p}\mathcal{P}_k^{XY,j-p} + |g_{l,k}^{XY}|^2\mathcal{P}_{k+l}^{XX,p}\mathcal{P}_k^{YY,j-p}),$$

where $\mathcal{P}_k^{XY,j} \equiv \sum_{p=0}^{j}\delta^p X_k \delta^{j-p}Y_k^*$ so that $\tilde{X}_k\tilde{Y}_k^* = \sum_{p=0}^{\infty}\mathcal{P}_k^{XY,p}$. Using the fact that $\langle\mathcal{O}_l^{(2j+1)}\rangle = \langle\mathcal{N}_l^{(2j+1)}\rangle = 0$ one then gets that

$$\langle|\hat{\phi}_l^{XY}|^2 - \delta_0 N_{l,\mathrm{obs}}^{(0)}\rangle = \sum_{j=0}^{\infty}\langle\mathcal{O}_l^{(2j)} - \delta_0\mathcal{N}_l^{(2j)}\rangle. \tag{16}$$

Now by defining $N_{l,\mathrm{obs}}^{(j)}$ for $j \geq 1$ as

$$N_{l,\mathrm{obs}}^{(j)} \equiv \begin{cases} \delta_0^{-1}\mathcal{O}_l^{(2j)} - \mathcal{N}_l^{(2j)} - C_l^{\phi\phi} & \text{when } j = 1 \\ \delta_0^{-1}\mathcal{O}_l^{(2j)} - \mathcal{N}_l^{(2j)} & \text{when } j > 1 \end{cases} \tag{17}$$

we have that

$$\langle|\hat{\phi}_l^{XY}|^2\rangle = \delta_0[C_l^{\phi\phi} + \langle N_{l,\mathrm{obs}}^{(0)}\rangle + \langle N_{l,\mathrm{obs}}^{(1)}\rangle + \cdots] + \langle\mathcal{O}_l^{(0)} - \delta_0\mathcal{N}_l^{(0)}\rangle \tag{18}$$

where $N_{l,\mathrm{obs}}^{(j)}$ is of order ϕ^{2j}. Therefore the order ϕ^{2j} term in the bias of $\delta_0^{-1}|\hat{\phi}_l^{XY}|^2 - N_{l,\mathrm{obs}}^{(0)}$ is given by $\langle N_{l,\mathrm{obs}}^{(j)}\rangle$ for $j \geq 1$.

Remark: Notice that the zero order term $\langle\mathcal{O}_l^{(0)} - \delta_0\mathcal{N}_l^{(0)}\rangle$ can be computed easily by first substituting $\delta^0 X$ and $\delta^0 Y$ for every occurrence of $\tilde{X}$ and $\tilde{Y}$ in $|\hat{\phi}_l^{XY}|^2 - N_{l,\mathrm{obs}}^{(0)}$. Then applying the expectation $\langle\cdot\rangle$, applying Wick's theorem and subsequently canceling like terms, the remainder results in

$$\langle\mathcal{O}_l^{(0)} - \delta_0\mathcal{N}_l^{(0)}\rangle = -\frac{[A_l^{XY}g_{l,-l/2}^{XY}]^2}{(2\pi)^2} \times [C_{l/2,\mathrm{exp}}^{XX}C_{l/2,\mathrm{exp}}^{YY} + (C_{l/2,\mathrm{exp}}^{XY})^2]$$

when $\boldsymbol{l} \neq 0$. Moreover, since this term does not depend on ϕ one can simply subtract it out of the estimator when using $\delta_0^{-1}|\hat{\phi}_l^{XY}|^2 - N_{l,\mathrm{obs}}^{(0)}$ for estimation.

B. The difference between $N_l^{(1)}$ and $\langle N_{l,\mathrm{obs}}^{(1)}\rangle$

By matching the right-hand side of Eq. (14) with the right-hand side of (7) one gets that $\delta_0 N_l^{(1)}$ equals $\langle\mathcal{O}_l^{(2)}\rangle$ minus $\delta_0 C_l^{\phi\phi}$ and any disconnected terms. In contrast, $\delta_0\langle N_{l,\mathrm{obs}}^{(1)}\rangle$ equals $\langle\mathcal{O}_l^{(2)}\rangle$ minus $\delta_0 C_l^{\phi\phi}$ and $\langle\delta_0\mathcal{N}_l^{(2)}\rangle$. Therefore the difference between $\delta_0 N_l^{(1)}$ and $\delta_0\langle N_{l,\mathrm{obs}}^{(1)}\rangle$ is the difference between $\langle\delta_0\mathcal{N}_l^{(2)}\rangle$ and the disconnected terms in $\langle\mathcal{O}_l^{(2)}\rangle$. By expanding $\delta_0\tilde{C}_{l,\mathrm{exp}}^{XY} = \sum_{p=0}^{\infty}\langle\mathcal{P}_l^{XY,p}\rangle$ in the definition of $\delta_0 N_l^{(0)}$ (which equals all the disconnected terms), and retaining only the order ϕ^2 terms (what remains equals all the disconnected terms in $\langle\mathcal{O}_l^{(2)}\rangle$) we get

$$\sum_{p=0}^{2}\delta_0^{-1}[A_l^{XY}]^2\int\frac{d^2\boldsymbol{k}}{(2\pi)^2}(g_{l,k}^{XY}g_{l,-k-l}^{XY}\langle\mathcal{P}_{k+l}^{XY,p}\rangle\langle\mathcal{P}_k^{XY,2-p}\rangle + |g_{l,k}^{XY}|^2\langle\mathcal{P}_{k+l}^{XX,p}\rangle\langle\mathcal{P}_k^{YY,2-p}\rangle). \tag{19}$$

Therefore the difference between $\delta_0 N_l^{(1)}$ and $\delta_0\langle N_{l,\mathrm{obs}}^{(1)}\rangle$ is given by the difference between (19) and $\langle\delta_0\mathcal{N}_l^{(2)}\rangle$ which equals

$$\sum_{p=0}^{2}\delta_0^{-1}[A_l^{XY}]^2\int\frac{d^2\boldsymbol{k}}{(2\pi)^2}(g_{l,k}^{XY}g_{l,-k-l}^{XY}\langle\mathcal{P}_{k+l}^{XY,p}\mathcal{P}_k^{XY,2-p}\rangle + |g_{l,k}^{XY}|^2\langle\mathcal{P}_{k+l}^{XX,p}\mathcal{P}_k^{YY,2-p}\rangle). \tag{20}$$

For the experimental conditions analyzed in this paper this difference is small.

V. FAST MONTE CARLO ALGORITHMS

In this section we give two simulation based methods for quickly estimating $N_l^{(j)}$ and $\langle N_{l,\mathrm{obs}}^{(j)}\rangle$ for $j \geq 0$. The first method simply observes that each term $\mathcal{L}_l^{(j)}$, $\mathcal{O}_l^{(j)}$ and $\mathcal{N}_l^{(j)}$ has fast Fourier transform characterizations which can be used for simulating $N_{l,\mathrm{obs}}^{(j)}$ and—by averaging multiple realizations—for estimating $\langle N_{l,\mathrm{obs}}^{(j)}\rangle$. This algorithm also extends to $N_l^{(j)}$ by replacing the expansion of $N_{l,\mathrm{obs}}^{(0)}$ in (15) with the corresponding expansion for $N_l^{(0)}$. The second method is exclusive to $N_l^{(1)}$ and uses correlated and uncorrelated CMB fields to mimic the appropriate Wick contractions for the connected terms in (8).

A. FFT algorithms for $N_{l,\mathrm{obs}}^{(j)}$ and $N_l^{(j)}$

The fast simulation techniques presented in this section depend on the fact that the transforms which characterize $\hat{\phi}_l^{XY}$ and $\tilde{\phi}_l^{XY}$ can be derived as Fourier transforms of pointwise products of gradients in pixel space. This was first utilized in [3,4] for the flat sky quadratic estimators. In the Appendix, we present these transforms along with some additional FFT transforms which allow fast simulation of the fields $\mathcal{L}_l^{(j)}$, $\mathcal{O}_l^{(j)}$ and $\mathcal{N}_l^{(j)}$. This is the basis of the algorithm which then uses Eq. (17) to simulate $N_{l,\mathrm{obs}}^{(j)}$.

For $\mathcal{L}_l^{(j)}$ and $\mathcal{O}_l^{(j)}$ first notice that each term $\delta^j X_l$ can be easily simulated in the pixel domain since $\delta^j X(\boldsymbol{x})$ is the pointwise product of derivatives of $X(\boldsymbol{x})$ and $\phi(\boldsymbol{x})$. Moreover the quadratic estimate applied to these terms, resulting in $A_l^{XY}\int\frac{d^2\boldsymbol{k}}{2\pi}g_{l,\boldsymbol{k}}^{XY}[\delta^p X_{\boldsymbol{k}+l}\delta^{j-p}Y_{\boldsymbol{k}}^*]$, is also easily computed by direct application of the formulas presented in the Appendix. Now summing over $p \in \{0,\ldots,j\}$ gives fast simulation of $\mathcal{L}_l^{(j)}$ which, in turn, gives $\mathcal{O}_l^{(j)}$ by taking quadratic combinations of $\mathcal{L}_l^{(0)},\ldots,\mathcal{L}_l^{(j)}$. Finally, to simulate $\mathcal{N}_l^{(j)}$ start by noticing that each term $\mathcal{P}_{\boldsymbol{k}}^{XY,j}\equiv\sum_{p=0}^{j}\delta^p X_{\boldsymbol{k}}\delta^{j-p}Y_{\boldsymbol{k}}^*$ simulates easily from $\delta^p X_{\boldsymbol{k}}$ and $\delta^{j-p}Y_{\boldsymbol{k}}^*$. Then to recover $\mathcal{N}_l^{(j)}$ one uses the FFT transformations presented in the Appendix for quick simulations of $[A_l^{XY}]^2\int\frac{d^2\boldsymbol{k}}{(2\pi)^2}g_{l,\boldsymbol{k}}^{XY}g_{l,-\boldsymbol{k}-l}^{XY}\mathcal{P}_{\boldsymbol{k}+l}^{XY,p}\mathcal{P}_{\boldsymbol{k}}^{XY,j-p}$ and $[A_l^{XY}]^2\times\int\frac{d^2\boldsymbol{k}}{(2\pi)^2}|g_{l,\boldsymbol{k}}^{XY}|^2\mathcal{P}_{\boldsymbol{k}+l}^{XX,p}\mathcal{P}_{\boldsymbol{k}}^{YY,2-p}$.

Monte Carlo averaging n independent simulations of $N_{l,\mathrm{obs}}^{(j)}$ will yield estimates of $\langle N_{l,\mathrm{obs}}^{(j)}\rangle$ with error bars that can be approximated by $s_l/\sqrt{n}$ where s_l denotes the standard deviation of the samples at each frequency $\boldsymbol{l}$. In addition, when the noise and beam structure are isotropic one can reduce the error bars by radially averaging each simulation of $N_{l,\mathrm{obs}}^{(j)}$. These error bars can then be used for refitting algorithms where $C_l^{\phi\phi}$ is iteratively fit to $\delta_0^{-1}|\hat{\phi}_l^{XY}|^2 - N_{l,\mathrm{obs}}^{(0)} - \mu_l$ where μ_l is an approximate bias correction based on the estimates of the higher order bias correction terms $\langle N_{l,\mathrm{obs}}^{(j)}\rangle$. Notice that for fast refitting algorithms, it may be advantageous initially to tolerate relatively large Monte Carlo error bars, and then iteratively increase the number of Monte Carlo samples at each refit.

We finally mention that the above simulation methods which are used to estimate $\langle N_{l,\mathrm{obs}}^{(j)}\rangle$ can also be used to estimate $N_l^{(j)}$. The only change is to replace each term $\mathcal{P}_{\boldsymbol{k}+l}^{XY,p}$, $\mathcal{P}_{\boldsymbol{k}}^{XY,2j-p}$, $\mathcal{P}_{\boldsymbol{k}+l}^{XX,p}$ and $\mathcal{P}_{\boldsymbol{k}}^{XX,2j-p}$ in the definition of $\mathcal{N}_l^{(2j)}$ with their respective expected values: $\langle\mathcal{P}_{\boldsymbol{k}+l}^{XY,p}\rangle$, $\langle\mathcal{P}_{\boldsymbol{k}}^{XY,2j-p}\rangle$, $\langle\mathcal{P}_{\boldsymbol{k}+l}^{XX,p}\rangle$ and $\langle\mathcal{P}_{\boldsymbol{k}}^{XX,2j-p}\rangle$.

B. Coupling lensing fields for $N_l^{(1)}$

A second algorithm, for Monte Carlo estimation of $N_l^{(1)}$, is to use correlated and uncorrelated CMB fields to mimic the Wick contraction structure appearing in the definition of $N_l^{(1)}$. The algorithm is easiest to illustrate with the EB quadratic estimator since the definition of $N_l^{(1)}$ only involves a small number of connected terms in (8) (when assuming a zero B mode in the unlensed CMB polarization field). The algorithm is derived by first noticing that the sum of the connected terms of order ϕ^2 in $\langle\hat{\phi}_l^{XY}\hat{\phi}_{l'}^{XY^*}\rangle$ is given by

$$\delta_{l-l'}\left[N_l^{(1)}+C_l^{\phi\phi}\right] = A_l^{XY}A_{l'}^{XY}\int\frac{d^2\boldsymbol{k}}{2\pi}\int\frac{d^2\boldsymbol{k}'}{2\pi}g_{l,\boldsymbol{k}}^{XY}g_{l',\boldsymbol{k}'}^{XY} \times\Big[\big\langle\delta^0E_{\boldsymbol{k}+l}\delta^1B_{\boldsymbol{k}}^*\delta^0E_{\boldsymbol{k}'+l'}^*\delta^1B_{\boldsymbol{k}'}\big\rangle + \big\langle\delta^0E_{\boldsymbol{k}+l}\delta^1B_{\boldsymbol{k}}^*\delta^0E_{\boldsymbol{k}'+l'}^*\delta^1B_{\boldsymbol{k}'}\big\rangle\Big]$$

These two Wick contraction terms have a Monte Carlo characterization as follows. Let (Q_l, U_l) and (Q_l', U_l') denote two independent realizations of the CMB polarization. Now let $\hat{\phi}_{l,1}^{EB}$ and $\hat{\phi}_{l,2}^{EB}$ denote the EB quadratic estimator applied to the pairs (E_l, δ^1B_l) and (E_l', δ^1B_l'), respectively, where δ^1B and δ^1B' use the same lensing potential ϕ so that

$$\delta^1B_l \equiv \sin(2\varphi_l)\delta^1Q_l - \cos(2\varphi_l)\delta^1U_l$$
$$\delta^1B_l' \equiv \sin(2\varphi_l)\delta^1Q_l' - \cos(2\varphi_l)\delta^1U_l'$$

where $\delta^1Q(\boldsymbol{x}) \equiv \nabla^a Q(\boldsymbol{x})\nabla_a\phi(\boldsymbol{x})$ and $\delta^1Q'(\boldsymbol{x}) \equiv \nabla^a Q'(\boldsymbol{x})\nabla_a\phi(\boldsymbol{x})$ [similar definitions for $\delta^1U(\boldsymbol{x})$ and $\delta^1U'(\boldsymbol{x})$]. Notice the independence structure of the simulated fields (that E and B are independent of E' and B') implies

$$\big\langle\hat{\phi}_{l,1}^{EB}\hat{\phi}_{l',2}^{EB^*}\big\rangle = A_l^{XY}A_{l'}^{XY}\int\frac{d^2\boldsymbol{k}}{2\pi}\int\frac{d^2\boldsymbol{k}'}{2\pi}g_{l,\boldsymbol{k}}^{XY}g_{l',\boldsymbol{k}'}^{XY} \times\big\langle\delta^0E_{\boldsymbol{k}+l}\delta^1B_{\boldsymbol{k}}^*\delta^0E_{\boldsymbol{k}'+l'}^*\delta^1B_{\boldsymbol{k}'}\big\rangle.$$

Similarly let $\hat{\phi}^{EB}_{l,3}$ and $\hat{\phi}^{EB}_{l,4}$ denote the EB quadratic estimator applied to the pairs $(E'_l, \delta^1 B_l)$ and $(E_l, \delta^1 B'_l)$ respectively (again using the same lensing potential ϕ). Then

$$\langle \hat{\phi}^{EB}_{l,3} \hat{\phi}^{EB^*}_{l',4} \rangle = A^{XY}_l A^{XY}_{l'} \int \frac{d^2\boldsymbol{k}}{2\pi} \int \frac{d^2\boldsymbol{k}'}{2\pi} g^{XY}_{l,\boldsymbol{k}} g^{XY}_{l',\boldsymbol{k}'} \times \langle \delta^0 E_{\boldsymbol{k}+\boldsymbol{l}} \delta^1 B^*_{\boldsymbol{k}} \delta^0 E^*_{\boldsymbol{k}'+\boldsymbol{l}'} \delta^1 B_{\boldsymbol{k}'} \rangle.$$

This leads to the following Monte Carlo averaging characterization of $N^{(1)}_l$:

$$N^{(1)}_l = \delta_0^{-1} \langle \hat{\phi}^{EB}_{l,1} \hat{\phi}^{EB^*}_{l,2} + \hat{\phi}^{EB}_{l,3} \hat{\phi}^{EB^*}_{l,4} \rangle - C^{\phi\phi}_l. \quad (21)$$

The above formula also holds for the lensed quadratic estimator $\tilde{\phi}^{EB}_l$ as well. It is easy to see that this method can be extended to all other polarization quadratic estimators, but with decidedly more connected terms.

Notice that there is an additional simplification when using the quadratic estimator, $\hat{\phi}^{EB}_l$, without lensed weights. In particular, $\delta_0^{-1} \langle \hat{\phi}^{EB}_{l,3} \hat{\phi}^{EB^*}_{l,4} \rangle = C^{\phi\phi}_l$ so that Eq. (21) simplifies to $N^{(1)}_l = \delta_0^{-1} \langle \hat{\phi}^{EB}_{l,1} \hat{\phi}^{EB^*}_{l,2} \rangle$. However, this simplification does not hold for $\tilde{\phi}^{EB}_l$ since the bias factor B^{EB}_l, defined in Sec. II A, implies $\delta_0^{-1} \langle \tilde{\phi}^{EB}_{l,3} \tilde{\phi}^{EB^*}_{l,4} \rangle = [B^{EB}_l]^2 C^{\phi\phi}_l \neq C^{\phi\phi}_l$.

One advantage of using this coupling technique is that the simulation of the $\delta^0 X$ and $\delta^0 Y$ can be done without including the additive experimental noise. To see why, notice that any CMB Wick contraction connecting $\delta^0 X$ and $\delta^0 Y$ (which depends on the additive experimental noise) must have bottom contraction symbols that connect $\delta^1 X$ and $\delta^1 Y$. This must yield a disconnected term which does not contribute to $N^{(1)}_l$.

VI. SIMULATION

We perform three simulation experiments under experimental conditions similar to those found in future ACTpol/SPTpol experiments. The first simulation explores the bias terms $N^{(j)}_l$ and $\langle N^{(j)}_{l,\mathrm{obs}} \rangle$ for the two quadratic estimators $\hat{\phi}^{XY}_l$ and $\tilde{\phi}^{XY}_l$. The results are summarized in Figs. 1–3. For these simulations, to compute the lensed weights in $\tilde{\phi}^{XY}_l$, we use the same fiducial model for $C^{\phi\phi}_l$ as the simulation model for $C^{\phi\phi}_l$. In contrast, for the second set of simulations we explore the effect of uncertainty in the fiducial model for $C^{\phi\phi}_l$ when computing $\tilde{\phi}^{XY}_l$. The results are summarized in Figs. 4–6. The main conclusion of the first set of simulations is that although $\tilde{\phi}^{XY}_l$ does reduce low l estimation bias, this is accomplished by increasing $N^{(1)}_l$ [or $\langle N^{(1)}_{l,\mathrm{obs}} \rangle$ in the case that one uses $N^{(0)}_{l,\mathrm{obs}}$ instead of $N^{(0)}_l$] to the point of canceling with $N^{(2)}_l$ [or $\langle N^{(2)}_{l,\mathrm{obs}} \rangle$ as the case may be] when the correct model for $C^{\phi\phi}_l$ is used to generate the lensed weights. The second set of simulations shows that this cancellation can be sensitive to the fiducial model for $C^{\phi\phi}_l$ depending on which estimator one uses: TE and EE are most sensitive; EB is least sensitive. Finally, for our third simulation, summarized in Figs. 7–9, we show that our estimates of $\langle N^{(1)}_{l,\mathrm{obs}} \rangle$ and $\langle N^{(2)}_{l,\mathrm{obs}} \rangle$ under a wrong fiducial

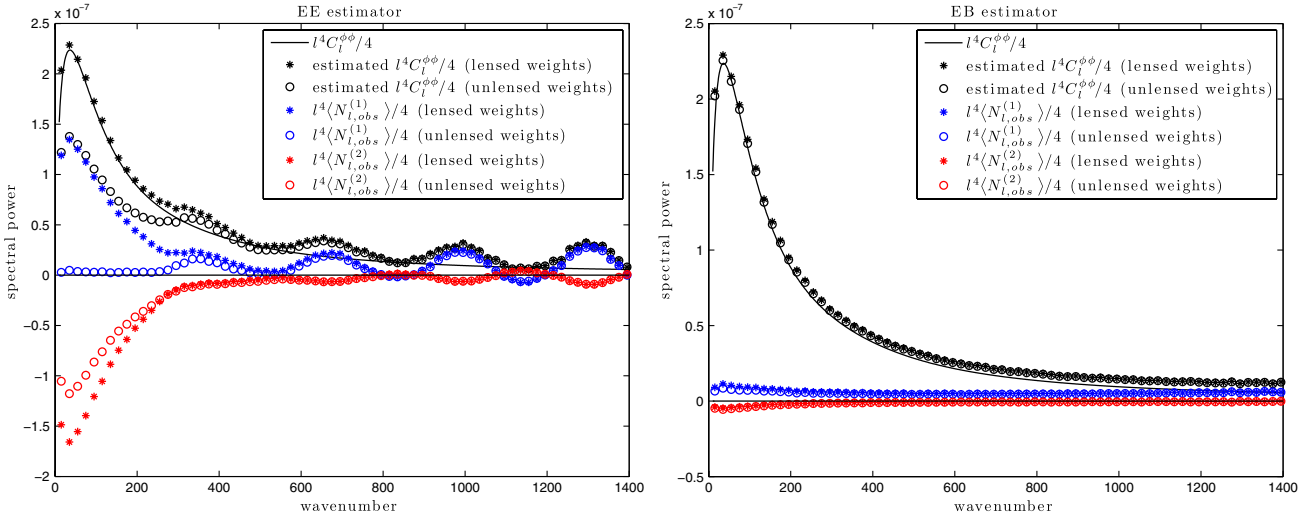

FIG. 1 (color online). These figures demonstrate the difference between EE and EB quadratic estimators when using lensed versus unlensed spectra into the estimator weights. The main feature of the left-hand plot is the reduction of bias—comparing $*$ with $\circ$—in the EE estimator when the lensed spectra are used for the estimator weights. Also by comparing $*$ with $\circ$ and $*$ with $\circ$ it is clear that this reduction is obtained by an increase in magnitude of both the so-called $N^{(1)}$ and $N^{(2)}$ bias to the extent that they nearly cancel. The first order bias term $l^4\langle N^{(1)}_{l,\mathrm{obs}} \rangle/4$ is denoted $*$ for $\tilde{\phi}^{XY}_l$ and $\circ$ for $\hat{\phi}^{XY}_l$. The second order bias term $l^4\langle N^{(2)}_{l,\mathrm{obs}} \rangle/4$ is denoted $*$ for $\tilde{\phi}^{XY}_l$ and $\circ$ for $\hat{\phi}^{XY}_l$. Finally, the expected value of the spectral density estimates $l^4\langle \delta_0^{-1} |\hat{\phi}^{XY}_l|^2 - N^{(0)}_{l,\mathrm{obs}} \rangle/4$ and $l^4\langle \delta_0^{-1} |\tilde{\phi}^{XY}_l|^2 - N^{(0)}_{l,\mathrm{obs}} \rangle/4$ are denoted by $\circ$ and $*$ respectively. See Sec. VI for details.

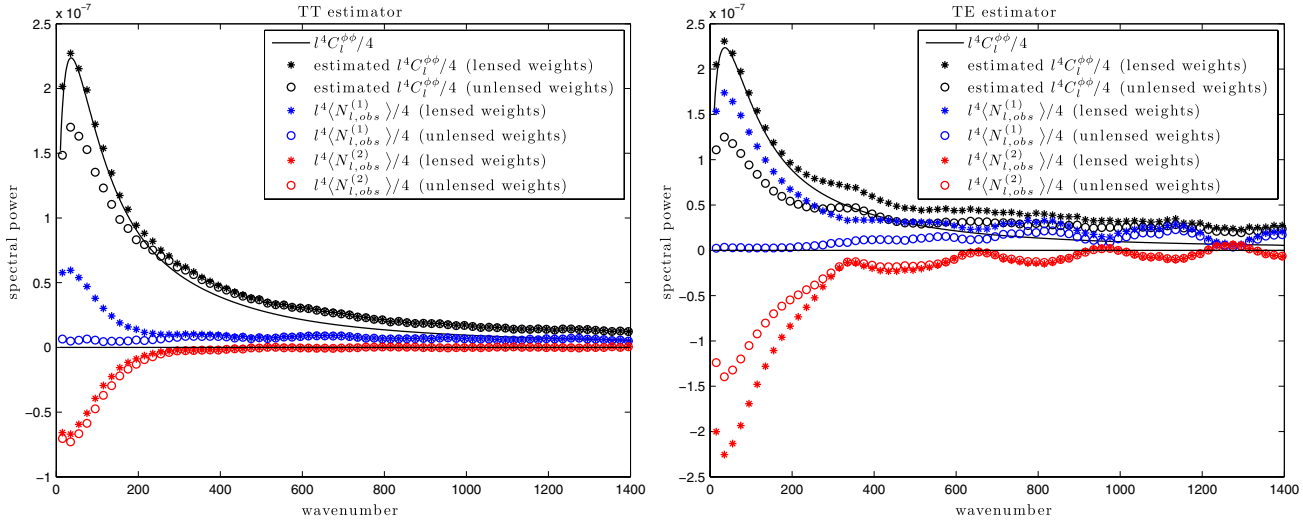

FIG. 2 (color online). The first order bias term $l^4\langle N^{(1)}_{l,\mathrm{obs}}\rangle/4$ is denoted $*$ for $\tilde{\phi}^{XY}_l$ and $\circ$ for $\hat{\phi}^{XY}_l$. The second order bias term $l^4\langle N^{(2)}_{l,\mathrm{obs}}\rangle/4$ is denoted $*$ for $\tilde{\phi}^{XY}_l$ and $\circ$ for $\hat{\phi}^{XY}_l$. Finally, the expected value of the spectral density estimates $l^4\langle\delta_0^{-1}|\hat{\phi}^{XY}_l|^2 - N^{(0)}_{l,\mathrm{obs}}\rangle/4$ and $l^4\langle\delta_0^{-1}|\tilde{\phi}^{XY}_l|^2 - N^{(0)}_{l,\mathrm{obs}}\rangle/4$ are denoted by $\circ$ and $*$ respectively. See Sec. VI for details.

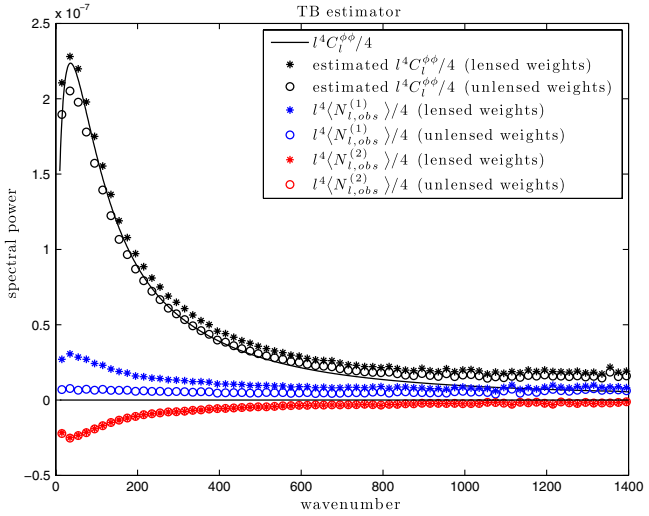

FIG. 3 (color online). The first order bias term $l^4\langle N^{(1)}_{l,\mathrm{obs}}\rangle/4$ is denoted $*$ for $\tilde{\phi}^{XY}_l$ and $\circ$ for $\hat{\phi}^{XY}_l$. The second order bias term $l^4\langle N^{(2)}_{l,\mathrm{obs}}\rangle/4$ is denoted $*$ for $\tilde{\phi}^{XY}_l$ and $\circ$ for $\hat{\phi}^{XY}_l$. Finally, the expected value of the spectral density estimates $l^4\langle\delta_0^{-1}|\hat{\phi}^{XY}_l|^2 - N^{(0)}_{l,\mathrm{obs}}\rangle/4$ and $l^4\langle\delta_0^{-1}|\tilde{\phi}^{XY}_l|^2 - N^{(0)}_{l,\mathrm{obs}}\rangle/4$ are denoted by $\circ$ and $*$ respectively. See Sec. VI for details.

for $C_l^{\phi\phi}$ can be used to successfully bias-correct the estimate of $C_l^{\phi\phi}$ based on $\tilde{\phi}^{XY}_l$ over a large range of $\boldsymbol{l}$.

The cosmology used in our simulations is based on a flat, power law ΛCDM cosmological model, with baryon density $\Omega_b = 0.044$; cold dark matter density $\Omega_{\mathrm{cdm}} = 0.21$; cosmological constant density $\Omega_\Lambda = 0.74$; Hubble parameter $h = 0.71$ in units of 100 km s^{-1} Mpc^{-1}; primordial scalar fluctuation amplitude $A_s(k = 0.002\ \mathrm{Mpc}^{-1}) = 2.45 \times 10^{-9}$; scalar spectral index $n_s(k = 0.002\ \mathrm{Mpc}^{-1}) = 0.96$; primordial helium abundance $Y_P = 0.24$; and reionization optical depth $\tau_r = 0.088$. The CAMB code is used to generate the theoretical power spectra [8].

To construct the lensed CMB simulation we first generate a high resolution simulation of $T(\boldsymbol{x})$, $Q(\boldsymbol{x})$ and $U(\boldsymbol{x})$ and the gravitational potential $\phi(\boldsymbol{x})$ on a periodic 25.6° × 25.6° patch of the flat sky. The lensing operation is performed by taking the numerical gradient of ϕ, then using linear interpolation to obtain the lensed fields $T(\boldsymbol{x} + \nabla\phi(\boldsymbol{x}))$, $Q(\boldsymbol{x} + \nabla\phi(\boldsymbol{x}))$ and $U(\boldsymbol{x} + \nabla\phi(\boldsymbol{x}))$. We downsample the lensed field to obtain the desired 1.5 arcmin pixel resolution for the simulation output. Finally, the observational noise (with a standard deviation of 5μK-arcmin on T and $\sqrt{2} \times 5\mu$K-arcmin on E, B and Gaussian beam FWHM = 1.5 arcmin deconvolution) is added in Fourier space. For all of the simulations we assume a zero B mode and a lensing potential ϕ which is uncorrelated with the CMB. In contrast to the full lensing simulation, the perturbative expansions given in Sec. V A only require simulation of unlensed CMB fields at the low resolution 1.5 arcmin pixels.

A. Figures 1–3

Each plot in Figs. 1–3 corresponds to a different quadratic pairing $X, Y \in \{T, E, B\}$ and shows the Monte Carlo approximations to $l^4\langle N^{(1)}_{l,\mathrm{obs}}\rangle/4$ and $l^4\langle N^{(2)}_{l,\mathrm{obs}}\rangle/4$ along with the expected value of the spectral density estimates $l^4(\delta_0^{-1}|\hat{\phi}^{XY}_l|^2 - N^{(0)}_{l,\mathrm{obs}})/4$ and $l^4(\delta_0^{-1}|\tilde{\phi}^{XY}_l|^2 - N^{(0)}_{l,\mathrm{obs}})/4$ over different realizations of ϕ, the CMB and the observational noise. Although not shown, the bias terms $l^4N^{(1)}_l/4$ were also computed, using the coupling technique given in Sec. V B, and resulted in very similar plots (mostly indistinguishable above the Monte Carlo error). The spectral

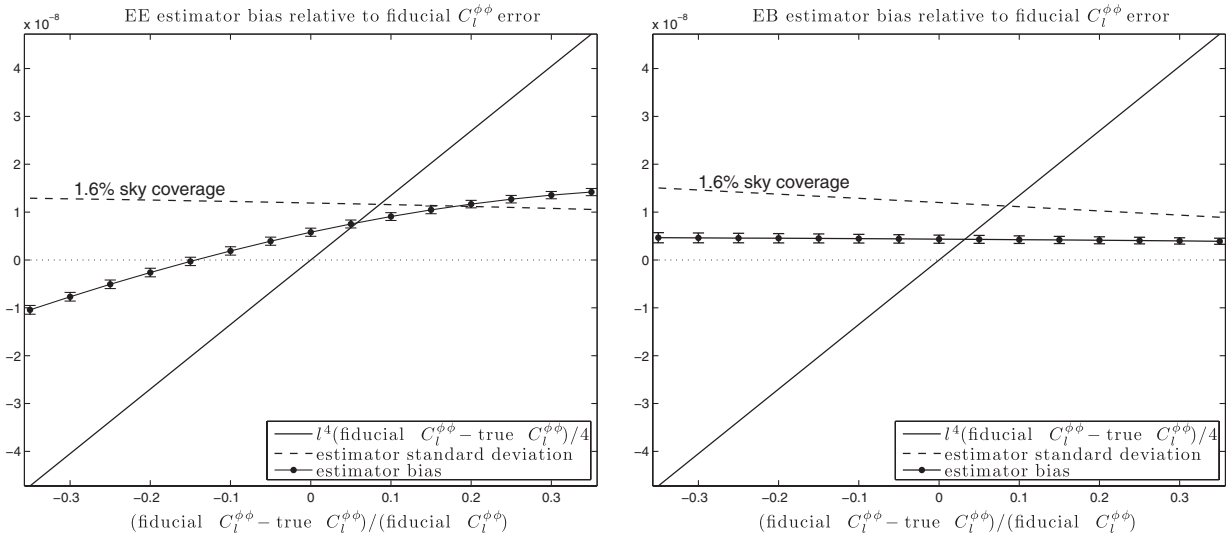

FIG. 4. Spectral estimation bias averaged over the multiple bin $l \in [10, 200]$ as a function of fiducial uncertainty. See Sec. VI for details.

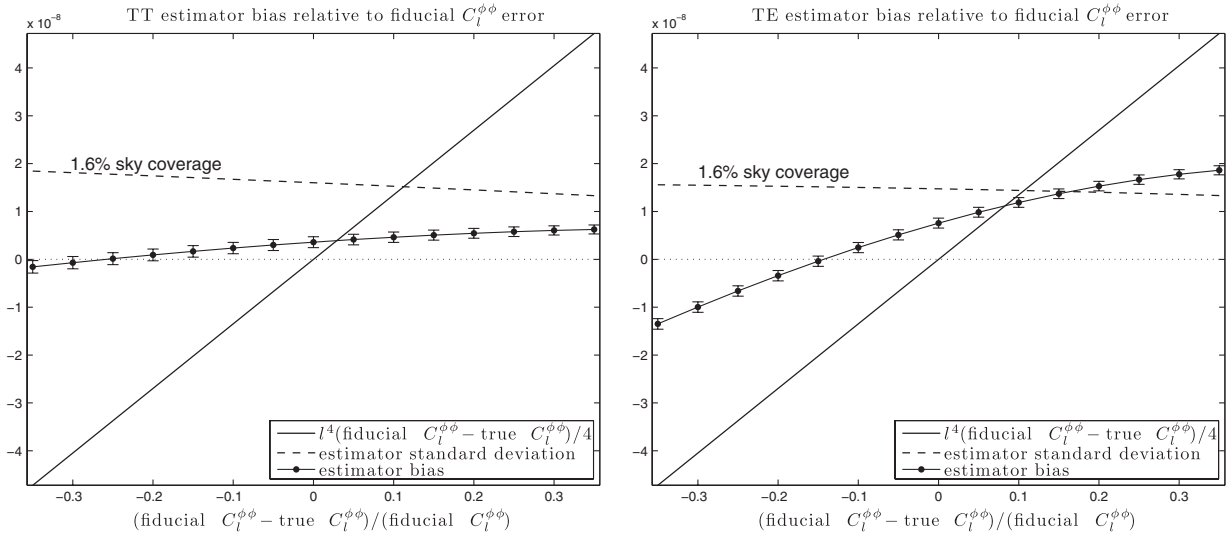

FIG. 5. Spectral estimation bias averaged over the multiple bin $l \in [10, 200]$ as a function of fiducial uncertainty. See Sec. VI for details.

density estimates are computed from the all-order lensed simulations whereas the bias terms are computed using perturbative expansions discussed in Sec. VA. The Monte Carlo approximations are based on 2000 independent realizations for the TT, EE and EB estimators and 18,000 independent realizations for the TE and TB estimators. These estimates are then radially averaged on sliding concentric annuli with wave number bins of width 20 to yield the plots shown in Figs. 1–3.

The main feature in these simulations is the large increase in $\langle N^{(1)}_{l,\mathrm{obs}}\rangle$ bias at low l for $\tilde{\phi}^{XY}_l$ as compared to the corresponding quantity for $\hat{\phi}^{XY}_l$, especially for the EE, TE and TT estimators. In contrast, $\langle N^{(2)}_{l,\mathrm{obs}}\rangle$ also increases in magnitude but to a lesser extent, enabling the cancellation with $\langle N^{(1)}_{l,\mathrm{obs}}\rangle$. Since the terms $\langle N^{(1)}_{l,\mathrm{obs}}\rangle$ and $\langle N^{(2)}_{l,\mathrm{obs}}\rangle$ are not individually small but instead cancel, there is the potential for this cancellation to be offset when there is uncertainty in the fiducial model for $C_l^{\phi\phi}$ used to compute the lensing weights for the estimate $\tilde{\phi}^{XY}_l$. In the next section we explore this sensitivity by analyzing the resulting estimation bias as a function of fiducial sensitivity.

B. Figures 4–6

For this set of simulations we analyze the effect of fiducial uncertainty when computing the lensed weights in the following estimate of $C_l^{\phi\phi}$:

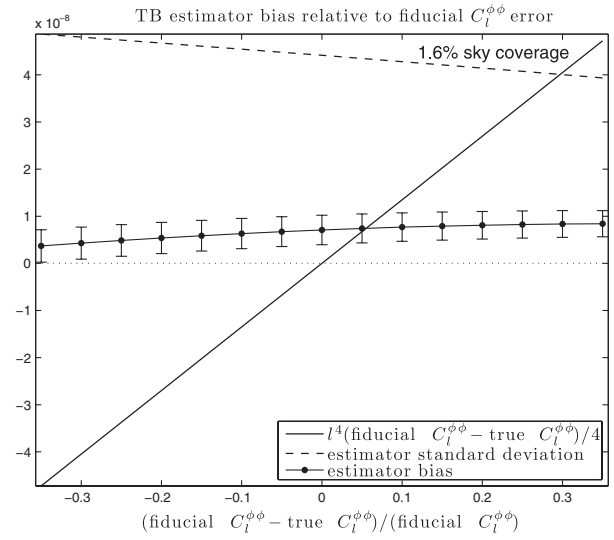

FIG. 6. Spectral estimation bias averaged over the multiple bin $l \in [10, 200]$ as a function of fiducial uncertainty. See Sec. VI for details.

$$\hat{C}_l^{\phi\phi} \equiv \delta_0^{-1}|\tilde{\phi}_l^{XY}|^2 - N_{l,\mathrm{obs}}^{(0)}.$$

In particular, we considered simulation models which differ from the fiducial model by a maximum of 35% only in the multipole range [10, 200]. The simulation models are of the form $T_l C_l^{\phi\phi}$ where $T_l = 1$ when $l \in [10, 200]$ and $T_l = c$ when $l \in [10, 200]$ where c ranges from 1.35 to 0.65. For each scalar c we simulated 200 different CMB, lensing and noise fields. At each simulation we recorded the estimation error, namely $l^4(\delta_0^{-1}|\tilde{\phi}_l^{XY}|^2 - N_{l,\mathrm{obs}}^{(0)} - T_l C_l^{\phi\phi})/4$, averaged over all frequencies in the l bin [10, 200]. This error is then averaged over all 200 simulations to estimate the bias. This bias is then plotted for each quadratic pairing $X, Y \in \{T, E, B\}$ in Figs. 4–6. The estimation bias is shown as $-\bullet-$ with 1σ monte carlo error bars attached as a function of the fiducial uncertainty $1 - c$ in the bin $l \in [10, 200]$. The dashed line shows the standard deviation of $l^4(\delta_0^{-1}|\tilde{\phi}_l^{XY}|^2 - N_{l,\mathrm{obs}}^{(0)})/4$ and the solid black line plots the fiducial error $(1 - T_l)l^4 C_l^{\phi\phi}/4$ averaged over $l \in [10, 200]$.

Table I summarizes fiducial uncertainty (at 15%), estimation standard deviation, and bias range when using $\tilde{\phi}_l^{XY}$ to estimate the average power in $l^4 C_l^{\phi\phi}/4$ over $l \in [10, 200]$. Each row corresponds to a different quadratic pairing $X, Y \in \{T, E, B\}$. The second column shows the bias range corresponding to 15% fiducial uncertainty taken from Figs. 4–6. We list bias range, versus absolute bias, since any baseline bias can be estimated with simulation and subsequently subtracted from any estimate. The third column shows 4σ full sky error bars where the estimation standard deviation is extrapolated from Figs. 4–6 to full sky σ by multiplying $\sqrt{f_{\mathrm{sky}}} = 0.126$. Notice that, ignoring the bias, the EE and EB estimator have the power to constrain the fiducial uncertainty by a factor of 3. However, accounting for bias this constraining power is mitigated, especially for estimators EE and TE. In contrast, the EB estimator bias can nearly be ignored completely.

C. Figures 7–9

The previous set of simulations demonstrated that fiducial uncertainty can affect inferential power at low multiple if unaccounted for. In the following set of simulations we consider subtracting out an estimate of the bias, using the

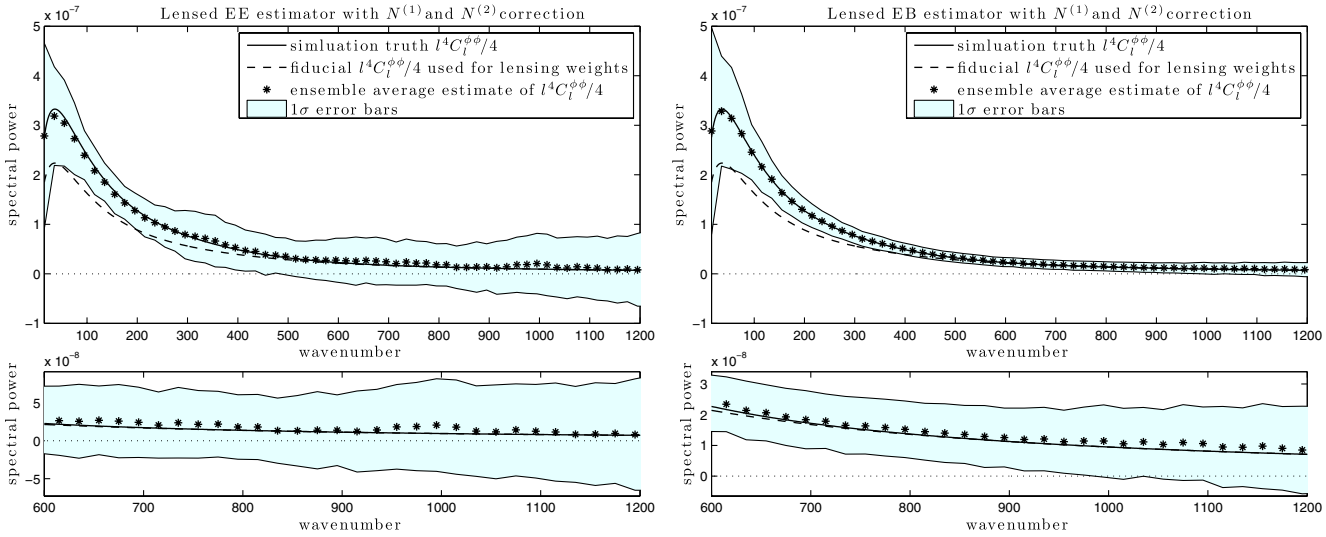

FIG. 7 (color online). The top plots show the average behavior of a bias-corrected estimate $\hat{C}_l^{\phi\phi}$, given in Eq. (22), based on $\tilde{\phi}_l^{EE}$ and $\tilde{\phi}_l^{EB}$. The fiducial model used to generate the corresponding lensed weights and $N^{(1)}$, $N^{(2)}$ is shown with a dashed line. The simulation truth used to generate the synthetic data is shown with a solid line. The bottom plots are simply magnified to the spectral range $l \in [200, 1200]$. See Sec. VI for details.

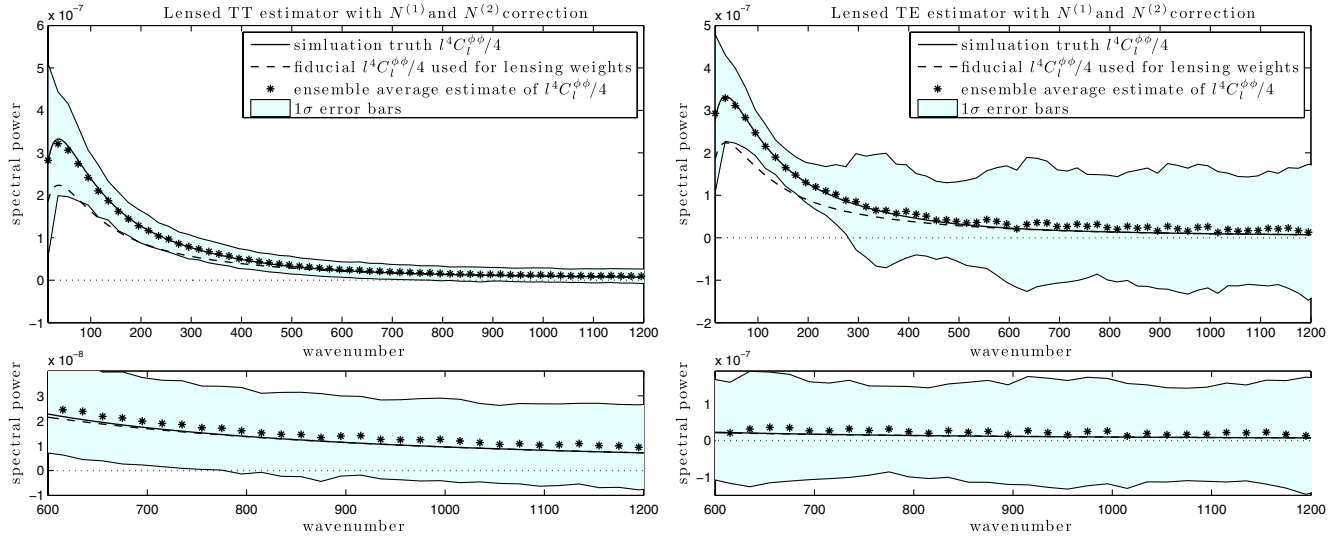

FIG. 8 (color online). The top plots show the average behavior of a bias-corrected estimate $\hat{C}_l^{\phi\phi}$, given in Eq. (22), based on $\tilde{\phi}_l^{TT}$ and $\tilde{\phi}_l^{TE}$. The fiducial model used to generate the corresponding lensed weights and $N^{(1)}$, $N^{(2)}$ is shown with a dashed line. The simulation truth used to generate the synthetic data is shown with a solid line. The bottom plots are simply magnified to the spectral range $l \in [200, 1200]$. See Sec. VI for details.

methods presented earlier, where we use a fiducial model to compute both the lensed weights and the $N^{(1)}$, $N^{(2)}$ bias. We demonstrate that this correction can be successful at removing bias, within estimation error, across a wide range of wave numbers.

The exact form of the bias-corrected estimate of $C_l^{\phi\phi}$ is defined as follows:

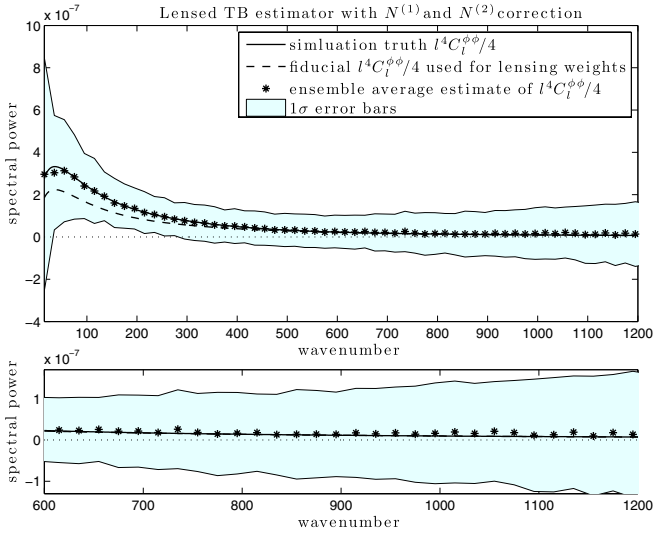

FIG. 9 (color online). The top plot shows the average behavior of a bias-corrected estimate $\hat{C}_l^{\phi\phi}$, given in Eq. (22), based on $\tilde{\phi}_l^{TB}$. The fiducial model used to generate the corresponding lensed weights and $N^{(1)}$, $N^{(2)}$ is shown with a dashed line. The simulation truth used to generate the synthetic data is shown with a solid line. The bottom plot is simply magnified to the spectral range $l \in [200, 1200]$. See Sec. VI for details.

$$\hat{C}_l^{\phi\phi} \equiv \delta_0^{-1}|\tilde{\phi}_l^{XY}|^2 - N_{l,\mathrm{obs}}^{(0)} - \langle N_{l,\mathrm{obs}}^{(1)} + N_{l,\mathrm{obs}}^{(2)}\rangle \qquad (22)$$

where the term $\langle N_{l,\mathrm{obs}}^{(1)} + N_{l,\mathrm{obs}}^{(2)}\rangle$ and the lensed weights in $\tilde{\phi}_l^{XY}$ are computed with a wrong fiducial model shown with a dashed line in Figs. 7–9. The simulation truth $C_l^{\phi\phi}$ is correspondingly shown with a solid line. Each simulation generates a synthetic data set from independent simulations of ϕ, T, E, B, along with observational noise. The estimate $\hat{C}_l^{\phi\phi}$ is then computed on each synthetic data set and is radially averaged on sliding concentric annuli with wave number bins of width 20. Finally, the radially averaged $\hat{C}_l^{\phi\phi}$ are averaged across each synthetic data set to generate a Monte Carlo approximation to $\langle\hat{C}_l^{\phi\phi}\rangle$. The results are shown with mark $*$ in Figs. 7–9. The main feature in these simulations is that the bias-corrected estimate $\hat{C}_l^{\phi\phi}$ is successful at removing bias across a wide range of wave numbers, even when using a relatively large error in the fiducial $C_l^{\phi\phi}$ model used for generating the lensed weights in $\tilde{\phi}_l^{XY}$ and the bias terms $\langle N_{l,\mathrm{obs}}^{(1)} + N_{l,\mathrm{obs}}^{(2)}\rangle$.

TABLE I. In units of spectral power, per 10^{-8}, the above table shows bias range, approximate full sky standard deviation and fiducial error (at 15%) for each quadratic estimate $\tilde{\phi}_l^{TE}$, $\tilde{\phi}_l^{EE}$, $\tilde{\phi}_l^{TT}$, $\tilde{\phi}_l^{TB}$ and $\tilde{\phi}_l^{EB}$.

$\tilde{\phi}_l^{XY}$	$\sim$ Bias range	$\sim$ Full sky 4σ	Fiducial error (15%)
TE	± 0.70	± 0.76	± 2.02
EE	± 0.53	± 0.62	± 2.02
TT	± 0.16	± 0.86	± 2.02
TB	± 0.10	± 2.33	± 2.02
EB	± 0.01	± 0.67	± 2.02

VII. DISCUSSION

The state-of-the-art estimator of weak lensing, the quadratic estimator developed by Hu and Okomoto [3,4], works in part through a delicate cancellation of terms in a Taylor expansion of the lensing effect on the CMB. In this paper we present two simulation based approaches for exploring the nature of this cancellation for both the CMB intensity and the polarization fields. In particular, we use these two simulation algorithms to analyze the so-called $N_l^{(1)}$ and $N_l^{(2)}$ bias for two modifications of the full set of quadratic temperature/polarization lensing estimators: one which incorporates lensed rather than unlensed spectra into the estimator weights to mitigate the effect of higher order terms; and one which uses the observed lensed CMB fields to correct for the, so-called, $N_l^{(0)}$ bias. Our simulation algorithms, which can simulate all higher order bias terms $N_l^{(j)}$ for $j \geq 0$, utilize an extension of the FFT techniques developed in [3]. These FFT characterizations are key to making estimates of the $N_l^{(j)}$ fast and additionally provide fast (nonstochastic) algorithms for approximating the $N_l^{(0)}$ bias using the observed lensed CMB fields.

In Sec. VI we use our algorithm to analyze the modified quadratic temperature/polarization lensing estimators for future ACTpol/SPTpol experiments. We find that the modified estimates do reduce low l estimation bias. However this is accomplished by effectively increasing the magnitude of $N_l^{(1)}$ and $N_l^{(2)}$ to the point of cancellation when the correct model for $C_l^{\phi\phi}$ is used to generate the lensed weights. We also demonstrate, through an analysis of estimator bias versus fiducial uncertainty, that this cancellation can be sensitive to the fiducial model for $C_l^{\phi\phi}$ depending on which estimator one uses: TE and EE are most sensitive; EB is least sensitive. For low l estimation in future ACTpol/SPTpol experiments we conclude that the bias in the EB estimator can be effectively ignored. For the TE and the EE estimators, however, the bias does contribute significantly to projected error bars and may need to be corrected to give the estimator inferential power beyond a nominal fiducial uncertainty.

ACKNOWLEDGMENTS

We gratefully acknowledge helpful suggestions from an anonymous referee and insightful discussions with D. Hanson, L. Knox and A. van Engelen. Supported by NSF Grants No. DMS-1007480 and No. DMS-1252795.

APPENDIX: FFT ALGORITHMS

In this section we derive the FFT algorithms which allow fast simulation of the fields $\mathcal{L}_l^{(j)}$, $\mathcal{O}_l^{(j)}$ and $\mathcal{N}_l^{(j)}$ as described in Sec. VA. We begin with some notational conventions which greatly simplify the subsequent formulas. First let $\varphi_{\boldsymbol{k}}$ denote the phase angle of frequency $\boldsymbol{k}$ and $\Delta\varphi \equiv \varphi_{\boldsymbol{k}+\boldsymbol{l}} - \varphi_{\boldsymbol{k}}$. Also let l_a denote the ath coordinate of $\boldsymbol{l}$. For any field $X \in \{T, E, B\}$ we let

$$\hat{X}_{\boldsymbol{k}} \equiv e^{i2\varphi_{\boldsymbol{k}}} X_{\boldsymbol{k}}, \qquad \check{X}_{\boldsymbol{k}} \equiv e^{i4\varphi_{\boldsymbol{k}}} X_{\boldsymbol{k}}.$$

Furthermore, we will utilize a superscript/subscript notation to denote multiplication/division by particular power spectra. An example serves to illustrate the notation:

$$(\check{X}_{TT})_{\boldsymbol{k}} \equiv \check{X}_{\boldsymbol{k}} \frac{1}{\tilde{C}^{TT}_{\boldsymbol{k},\mathrm{exp}}}, \qquad (\check{X}^{TE}_{TT,EE})_{\boldsymbol{k}} \equiv \check{X}_{\boldsymbol{k}} \frac{C^{TE}_{\boldsymbol{k}}}{\tilde{C}^{TT}_{\boldsymbol{k},\mathrm{exp}} \tilde{C}^{EE}_{\boldsymbol{k},\mathrm{exp}}}$$
$$(\check{X}^{TE}_{TT})_{\boldsymbol{k}} \equiv \check{X}_{\boldsymbol{k}} \frac{C^{TE}_{\boldsymbol{k}}}{\tilde{C}^{TT}_{\boldsymbol{k},\mathrm{exp}}}, \qquad (\check{X}^{TE,TT}_{TT,EE})_{\boldsymbol{k}} \equiv \check{X}_{\boldsymbol{k}} \frac{C^{TE}_{\boldsymbol{k}} C^{TT}_{\boldsymbol{k}}}{\tilde{C}^{TT}_{\boldsymbol{k},\mathrm{exp}} \tilde{C}^{EE}_{\boldsymbol{k},\mathrm{exp}}}.$$

Notice that the above denominators always use lensed spectra with experimental noise, whereas the numerators always use unlensed spectra. In doing so, the formulas found in claims 1 through 5 below can be used for fast algorithms for the quadratic estimate $\hat{\phi}_l^{XY}$. To obtain the corresponding formulas for the modified quadratic estimate $\tilde{\phi}_l^{XY}$ one simply needs to replace the unlensed spectra in the numerator of the above notation, with the lensed spectra (but without experimental noise).

Claim 1 (TT estimator) If $X_{\boldsymbol{k}}$ and $Y_{\boldsymbol{k}}$ are complex functions such that $X_{-\boldsymbol{k}} = X_{\boldsymbol{k}}^*$ and $Y_{-\boldsymbol{k}} = Y_{\boldsymbol{k}}^*$ then

$$\int \frac{d^2\boldsymbol{k}}{2\pi} g^{TT}_{l,k} X_{\boldsymbol{k}+\boldsymbol{l}} Y^*_{\boldsymbol{k}} = -il_a \int \frac{d^2\boldsymbol{x}}{2\pi} e^{-i\boldsymbol{l}\cdot\boldsymbol{x}} ([\nabla^a X^{TT}_{TT}(\boldsymbol{x})][Y_{TT}(\boldsymbol{x})] + [\nabla^a Y^{TT}_{TT}(\boldsymbol{x})][X_{TT}(\boldsymbol{x})]);$$

$$\int \frac{d^2\boldsymbol{k}}{(2\pi)^2} |g^{TT}_{l,k}|^2 X_{\boldsymbol{k}+\boldsymbol{l}} Y^*_{\boldsymbol{k}} = -\frac{l_a l_b}{2\pi} \int \frac{d^2\boldsymbol{x}}{2\pi} e^{-i\boldsymbol{l}\cdot\boldsymbol{x}} (2[\nabla^a X^{TT}_{TT,TT}(\boldsymbol{x})][\nabla^b Y^{TT}_{TT,TT}(\boldsymbol{x})] + [X_{TT,TT}(\boldsymbol{x})][\nabla^a\nabla^b Y^{TT,TT}_{TT,TT}(\boldsymbol{x})]$$
$$+ [Y_{TT,TT}(\boldsymbol{x})][\nabla^a\nabla^b X^{TT,TT}_{TT,TT}(\boldsymbol{x})]);$$

$$\int \frac{d^2\boldsymbol{k}}{(2\pi)^2} g^{TT}_{l,k} g^{TT}_{l,-\boldsymbol{k}-\boldsymbol{l}} X_{\boldsymbol{k}+\boldsymbol{l}} Y^*_{\boldsymbol{k}} = \int \frac{d^2\boldsymbol{k}}{(2\pi)^2} |g^{TT}_{l,k}|^2 X_{\boldsymbol{k}+\boldsymbol{l}} Y^*_{\boldsymbol{k}},$$

where $g^{TT}_{l,k} \equiv 2\pi f^{TT}_{l,k} [\tilde{C}^{TT}_{\boldsymbol{k}+\boldsymbol{l},\mathrm{exp}} \tilde{C}^{TT}_{\boldsymbol{k},\mathrm{exp}}]^{-1}$ and $f^{TT}_{l,k} \equiv \frac{1}{2\pi}[\boldsymbol{l}\cdot(\boldsymbol{k}+\boldsymbol{l})C^{TT}_{\boldsymbol{k}+\boldsymbol{l}} - \boldsymbol{l}\cdot\boldsymbol{k}C^{TT}_{\boldsymbol{k}}]$.

Claim 2 (TE estimator) If $X_{\boldsymbol{k}}$ and $Y_{\boldsymbol{k}}$ are complex functions such that $X_{-\boldsymbol{k}} = X_{\boldsymbol{k}}^*$ and $Y_{-\boldsymbol{k}} = Y_{\boldsymbol{k}}^*$ then

$$\int \frac{d^2\boldsymbol{k}}{2\pi} g^{TE}_{l,k} X_{k+l} Y^*_k = -il_a \int \frac{d^2\boldsymbol{x}}{2\pi} e^{-i\boldsymbol{l}\cdot\boldsymbol{x}} (\mathrm{Re}\{[\nabla^a \hat{X}^{TE}_{TT}(\boldsymbol{x})][\hat{Y}_{EE}(\boldsymbol{x})]^*\} + [\nabla^a Y^{TE}_{EE}(\boldsymbol{x})][X_{TT}(\boldsymbol{x})]);$$

$$\begin{aligned}\int \frac{d^2\boldsymbol{k}}{(2\pi)^2} |g^{TE}_{l,k}|^2 X_{k+l} Y^*_k = &-\frac{l_a l_b}{4\pi} \int \frac{d^2\boldsymbol{x}}{2\pi} e^{-i\boldsymbol{l}\cdot\boldsymbol{x}} ([Y_{EE,EE}(\boldsymbol{x})][\nabla^a\nabla^b X^{TE,TE}_{TT,TT}(\boldsymbol{x})] + \mathrm{Re}\{[\check{Y}_{EE,EE}(\boldsymbol{x})][\nabla^a\nabla^b \check{X}^{TE,TE}_{TT,TT}(\boldsymbol{x})]^*\} \\ &+ 2[X_{TT,TT}(\boldsymbol{x})][\nabla^a\nabla^b Y^{TE,TE}_{EE,EE}(\boldsymbol{x})] + \mathrm{Re}\{4[\nabla^a \hat{X}^{TE}_{TT,TT}(\boldsymbol{x})][\nabla^b \hat{Y}^{TE}_{EE,EE}(\boldsymbol{x})]^*\});\end{aligned}$$

$$\begin{aligned}\int \frac{d^2\boldsymbol{k}}{(2\pi)^2} g^{TE}_{l,k} g^{TE}_{l,-\boldsymbol{k}-\boldsymbol{l}} X_{k+l} Y^*_k = &-\frac{l_a l_b}{4\pi} \int \frac{d^2\boldsymbol{x}}{2\pi} e^{-i\boldsymbol{l}\cdot\boldsymbol{x}} (\mathrm{Re}\{2[\nabla^a\nabla^b \hat{X}^{TE,TE}_{TT,EE}(\boldsymbol{x})][\hat{Y}_{TT,EE}(\boldsymbol{x})]^*\} + \mathrm{Re}\{2[\nabla^a\nabla^b \hat{Y}^{TE,TE}_{TT,EE}(\boldsymbol{x})][\hat{X}_{TT,EE}(\boldsymbol{x})]^*\} \\ &+ 3[\nabla^a X^{TE}_{TT,EE}(\boldsymbol{x})][\nabla^b Y^{TE}_{TT,EE}(\boldsymbol{x})] + \mathrm{Re}\{[\nabla^b \check{Y}^{TE}_{TT,EE}(\boldsymbol{x})][\nabla^a \check{X}^{TE}_{TT,EE}(\boldsymbol{x})]^*\}),\end{aligned}$$

where $g^{TE}_{l,k} \equiv 2\pi f^{TE}_{l,k} [\tilde{C}^{TT}_{\boldsymbol{k}+\boldsymbol{l},\mathrm{exp}} \tilde{C}^{EE}_{\boldsymbol{k},\mathrm{exp}}]^{-1}$ and $f^{TE}_{l,k} \equiv \frac{1}{2\pi}[\boldsymbol{l}\cdot(\boldsymbol{k}+\boldsymbol{l})\cos(2\Delta\varphi) C^{TE}_{\boldsymbol{k}+\boldsymbol{l}} - \boldsymbol{l}\cdot\boldsymbol{k} C^{TE}_{\boldsymbol{k}}]$.

Claim 3 (TB estimator) If $X_{\boldsymbol{k}}$ and $Y_{\boldsymbol{k}}$ are complex functions such that $X_{-\boldsymbol{k}} = X^*_{\boldsymbol{k}}$ and $Y_{-\boldsymbol{k}} = Y^*_{\boldsymbol{k}}$ then

$$\int \frac{d^2\boldsymbol{k}}{2\pi} g^{TB}_{l,k} X_{k+l} Y^*_k = -il_a \int \frac{d^2\boldsymbol{x}}{2\pi} e^{-i\boldsymbol{l}\cdot\boldsymbol{x}} \mathrm{Im}\{[\nabla^a \hat{X}^{TE}_{TT}(\boldsymbol{x})][\hat{Y}_{BB}(\boldsymbol{x})]^*\};$$

$$\int \frac{d^2\boldsymbol{k}}{(2\pi)^2} |g^{TB}_{l,k}|^2 X_{k+l} Y^*_k = -\frac{l_a l_b}{4\pi} \int \frac{d^2\boldsymbol{x}}{2\pi} e^{-i\boldsymbol{l}\cdot\boldsymbol{x}} ([Y_{BB,BB}(\boldsymbol{x})][\nabla^a\nabla^b X^{TE,TE}_{TT,TT}(\boldsymbol{x})] - \mathrm{Re}\{[\check{Y}_{BB,BB}(\boldsymbol{x})][\nabla^a\nabla^b \check{X}^{TE,TE}_{TT,TT}(\boldsymbol{x})]^*\});$$

$$\int \frac{d^2\boldsymbol{k}}{(2\pi)^2} g^{TB}_{l,k} g^{TB}_{l,-\boldsymbol{k}-\boldsymbol{l}} X_{k+l} Y^*_k = -\frac{l_a l_b}{4\pi} \int \frac{d^2\boldsymbol{x}}{2\pi} e^{-i\boldsymbol{l}\cdot\boldsymbol{x}} ([\nabla^a X^{TE}_{TT,BB}(\boldsymbol{x})][\nabla^b Y^{TE}_{TT,BB}(\boldsymbol{x})] - \mathrm{Re}\{[\nabla^a \check{X}^{TE}_{TT,BB}(\boldsymbol{x})][\nabla^b \check{Y}^{TE}_{TT,BB}(\boldsymbol{x})]^*\}),$$

where $g^{TB}_{l,k} \equiv 2\pi f^{TB}_{l,k} [\tilde{C}^{TT}_{\boldsymbol{k}+\boldsymbol{l},\mathrm{exp}} \tilde{C}^{BB}_{\boldsymbol{k},\mathrm{exp}}]^{-1}$ and $f^{TB}_{l,k} \equiv \frac{1}{2\pi}[\boldsymbol{l}\cdot(\boldsymbol{k}+\boldsymbol{l}) C^{TE}_{\boldsymbol{k}+\boldsymbol{l}}] \sin(2\Delta\varphi)$.

Claim 4 (EB estimator) If $X_{\boldsymbol{k}}$ and $Y_{\boldsymbol{k}}$ are complex functions such that $X_{-\boldsymbol{k}} = X^*_{\boldsymbol{k}}$ and $Y_{-\boldsymbol{k}} = Y^*_{\boldsymbol{k}}$ then

$$\int \frac{d^2\boldsymbol{k}}{2\pi} g^{EB}_{l,k} X_{k+l} Y^*_k = -il_a \int \frac{d^2\boldsymbol{x}}{2\pi} e^{-i\boldsymbol{l}\cdot\boldsymbol{x}} \mathrm{Im}\{[\nabla^a \hat{X}^{EE}_{EE}(\boldsymbol{x})][\hat{Y}_{BB}(\boldsymbol{x})]^*\};$$

$$\int \frac{d^2\boldsymbol{k}}{(2\pi)^2} |g^{EB}_{l,k}|^2 X_{k+l} Y^*_k = -\frac{l_a l_b}{4\pi} \int \frac{d^2\boldsymbol{x}}{2\pi} e^{-i\boldsymbol{l}\cdot\boldsymbol{x}} ([Y_{BB,BB}(\boldsymbol{x})][\nabla^a\nabla^b X^{EE,EE}_{EE,EE}(\boldsymbol{x})] - \mathrm{Re}\{[\check{Y}_{BB,BB}(\boldsymbol{x})][\nabla^a\nabla^b \check{X}^{EE,EE}_{EE,EE}(\boldsymbol{x})]^*\});$$

$$\int \frac{d^2\boldsymbol{k}}{(2\pi)^2} g^{EB}_{l,k} g^{EB}_{l,-\boldsymbol{k}-\boldsymbol{l}} X_{k+l} Y^*_k = -\frac{l_a l_b}{4\pi} \int \frac{d^2\boldsymbol{x}}{2\pi} e^{-i\boldsymbol{l}\cdot\boldsymbol{x}} ([\nabla^a X^{EE}_{EE,BB}(\boldsymbol{x})][\nabla^b Y^{EE}_{EE,BB}(\boldsymbol{x})] - \mathrm{Re}\{[\nabla^a \check{X}^{EE}_{EE,BB}(\boldsymbol{x})][\nabla^b \check{Y}^{EE}_{EE,BB}(\boldsymbol{x})]^*\}),$$

where $g^{EB}_{l,k} \equiv 2\pi f^{EB}_{l,k} [\tilde{C}^{EE}_{\boldsymbol{k}+\boldsymbol{l},\mathrm{exp}} \tilde{C}^{BB}_{\boldsymbol{k},\mathrm{exp}}]^{-1}$ and $f^{EB}_{l,k} \equiv \frac{1}{2\pi}[\boldsymbol{l}\cdot(\boldsymbol{k}+\boldsymbol{l}) C^{EE}_{\boldsymbol{k}+\boldsymbol{l}}] \sin(2\Delta\varphi)$.

Claim 5 (EE estimator) If $X_{\boldsymbol{k}}$ and $Y_{\boldsymbol{k}}$ are complex functions such that $X_{-\boldsymbol{k}} = X^*_{\boldsymbol{k}}$ and $Y_{-\boldsymbol{k}} = Y^*_{\boldsymbol{k}}$ then

$$\int \frac{d^2\boldsymbol{k}}{2\pi} g^{EE}_{l,k} X_{k+l} Y^*_k = -il_a \int \frac{d^2\boldsymbol{x}}{2\pi} e^{-i\boldsymbol{l}\cdot\boldsymbol{x}} (\mathrm{Re}\{[\nabla^a \hat{X}^{EE}_{EE}(\boldsymbol{x})][\hat{Y}_{EE}(\boldsymbol{x})]^*\} + \mathrm{Re}\{[\nabla^a \hat{Y}^{EE}_{EE}(\boldsymbol{x})][\hat{X}_{EE}(\boldsymbol{x})]^*\});$$

$$\begin{aligned}\int \frac{d^2\boldsymbol{k}}{(2\pi)^2} |g^{EE}_{l,k}|^2 X_{k+l} Y^*_k = &-\frac{l_a l_b}{4\pi} \int \frac{d^2\boldsymbol{x}}{2\pi} e^{-i\boldsymbol{l}\cdot\boldsymbol{x}} ([\nabla^a\nabla^b X^{EE,EE}_{EE,EE}(\boldsymbol{x})][Y_{EE,EE}(\boldsymbol{x})] + \mathrm{Re}\{[\nabla^a\nabla^b \check{X}^{EE,EE}_{EE,EE}(\boldsymbol{x})][\check{Y}_{EE,EE}(\boldsymbol{x})]^*\} \\ &+ [X_{EE,EE}(\boldsymbol{x})][\nabla^a\nabla^b Y^{EE,EE}_{EE,EE}(\boldsymbol{x})] + \mathrm{Re}\{[\check{X}_{EE,EE}(\boldsymbol{x})][\nabla^a\nabla^b \check{Y}^{EE,EE}_{EE,EE}(\boldsymbol{x})]^*\} \\ &+ 2[\nabla^a X^{EE}_{EE,EE}(\boldsymbol{x})][\nabla^b Y^{EE}_{EE,EE}(\boldsymbol{x})] + \mathrm{Re}\{2[\nabla^a \check{X}^{EE}_{EE,EE}(\boldsymbol{x})][\nabla^b \check{Y}^{EE}_{EE,EE}(\boldsymbol{x})]^*\});\end{aligned}$$

$$\int \frac{d^2\boldsymbol{k}}{(2\pi)^2} g^{EE}_{l,k} g^{EE}_{l,-\boldsymbol{k}-\boldsymbol{l}} X_{k+l} Y^*_k = \int \frac{d^2\boldsymbol{k}}{(2\pi)^2} |g^{EE}_{l,k}|^2 X_{k+l} Y^*_k,$$

where $g^{EE}_{l,k} \equiv 2\pi f^{EE}_{l,k} [\tilde{C}^{EE}_{\boldsymbol{k}+\boldsymbol{l},\mathrm{exp}} \tilde{C}^{EE}_{\boldsymbol{k},\mathrm{exp}}]^{-1}$ and $f^{EE}_{l,k} \equiv \frac{1}{2\pi}[\boldsymbol{l}\cdot(\boldsymbol{k}+\boldsymbol{l}) C^{EE}_{\boldsymbol{k}+\boldsymbol{l}} - \boldsymbol{l}\cdot\boldsymbol{k} C^{EE}_{\boldsymbol{k}}] \cos(2\Delta\varphi)$.

[1] S. Das *et al.*, Phys. Rev. Lett. **107**, 021301 (2011).
[2] A. van Engelen *et al.*, Astrophys. J. **756**, 142 (2012).
[3] W. Hu, Astrophys. J. **557**, L79 (2001).
[4] W. Hu and T. Okamoto, Astrophys. J. **574**, 566 (2002).
[5] M. Kesden, A. Cooray, and M. Kamionkowski, Phys. Rev. D **67**, 123507 (2003).
[6] D. Hanson, A. Challinor, G. Efstathiou, and P. Bielewicz, Phys. Rev. D **83**, 043005 (2011).
[7] S. Dodelson, *Modern Cosmology* (Academic Press, New York, 2003).
[8] A. Lewis, A. Challinor, and A. Lasenby, Astrophys. J. **538**, 473 (2000).